Light-based vat-polymerization bioprinting

Riccardo Levato^{1,2,†} Oksana Dudaryeva², Carlos Ezio Garciamendez-Mijares³, Bruce E. Kirkpatrick^{4,5,6}, Riccardo Rizzo⁷, Jacob Schimelman⁸, Kristi S. Anseth^{4,5}, Shaochen Chen⁸, Marcy Zenobi-Wong⁷, Yu Shrike Zhang^{3,†}

6 7

8

- ¹Department of Clinical Sciences, Faculty of Veterinary Medicine, Utrecht University, Utrecht, The Netherlands
- ²Department of Orthopedics, University Medical Center Utrecht, Utrecht, The Netherlands
- ³Division of Engineering in Medicine, Brigham and Women's Hospital, Department of Medicine,
 Harvard Medical School, Cambridge, MA 02139, USA
- ⁴Department of Chemical and Biological Engineering, University of Colorado Boulder, Boulder, CO 80303, USA
 - ⁵BioFrontiers Institute, University of Colorado Boulder, Boulder, CO 80303, USA
- ⁶Medical Scientist Training Program, University of Colorado Anschutz Medical Campus, Aurora
 CO 80045, USA
- ⁷Department of Health Sciences and Technology, ETH Zürich, Zürich, Switzerland
 - ⁸Department of NanoEngineering, University of California San Diego, La Jolla, CA 92093, USA

18 19 20

14

†Emails: r.levato@uu.nl (R. L.); yszhang@research.bwh.harvard.edu (Y. S. Z.)

Abstract | Light-based vat-polymerization bioprinting enables computer-aided patterning of three-dimensional (3D) cell-laden structures in a point-by-point, layer-by-layer, or volumetric manner, through the use of vat(s) filled with bioresin(s) that are photoactivatable. This collection of technologies, divided by their modes of operation into stereolithography, digital light processing, and volumetric additive manufacturing, have been extensively developed over the last decades, leading to broad applications in biomedicine. In this Primer, we illustrate the methodology of light-based vat-polymerization 3D bioprinting from the perspectives of hardware, software, and bioresin selections. We follow with discussions on methodological variations of these technologies including their latest advancements, as well as elaborating on key assessments utilized towards ensuring qualities of the bioprinting procedures and products. We conclude by providing insights into future directions of light-based vat-polymerization methods.

[H1] Introduction

Three-dimensional (3D) bioprinting utilizes computer-aided processes to spatially pattern cells or/and auxiliary biomaterials to enable creation of functional bioengineered structures for a variety of applications in biomedicine¹⁻⁶. Light-based vat-polymerization was the first 3D printing method developed, back in 1986 in the form of stereolithography (SLA)⁷. Nevertheless, its biomedical utility^{8,9}, and in particular, expansion into bioprinting, *i.e.*, with cell loading into photopolymerizable hydrogels during the printing procedure, was not demonstrated until almost two decades later¹⁰.

Over the years, light-based vat-polymerization bioprinting has witnessed significant advancements across all aspects, through hardware optimizations to biomaterial designs and downstream applications. According to modes of operation, this collection of technologies can be divided into those that pattern the bioresin point-by-point, layer-by-layer, or directly volumetric; the specific modalities include lithographic techniques, such as stereolithography in its original implementation, utilizing single-photon lasers (SLA)^{11,12}, multi-photon polymerization lithography (MPL; oftentimes adopting the two-photon mechanism, or TPL)^{12,13}, digital light processing (DLP)^{11,12}, and volumetric bioprinting, also termed volumetric additive manufacturing (VAM)¹⁴⁻¹⁶. Despite these variations, a common feature of light-based vat-polymerization bioprinting methods is that they all rely on patterned light-dose distributions to initiate localized chemical reactions of photoactivatable bioresins. As the bioresins react in response to light, this results in the formation of desired structures in two-dimensions (2D) and in 3D volumes. While in most scenarios such chemical reactions are in the additive manner (i.e., photocrosslinking), they can also be made subtractive such as with photodegradation¹⁷. Different modalities for shaping light in enabling layer-by-layer or volumetric development of these photoreactions exist, each spanning a defined range of resolution, speed of fabrication, required bioresin properties, and therefore target applications.

This Primer intends to provide a thorough understanding of light-based vat-polymerization bioprinting, which forms a complementary toolset to another class of commonly used bioprinting methods relying on extrusion¹⁸. We present key considerations when selecting a light-based vat-polymerization bioprinting modality, relating to its hardware, software, and bioresin designs. We further describe assessments that are essential to ensure robust bioprinting procedures, reporting requirements to maximize reproducibility, as well as limitations of current technologies and improvements that can be made to mitigate these limitations. We finally conclude with future perspectives that involve discussions relating to integration of machine-learning and translations.

[H1] Experimentation

Light-based vat-polymerization bioprinting, compared to extrusion bioprinting¹⁸, generally provides improved controllability over structural complexity of the tissue constructs that can be produced at a faster fabrication rate and higher resolutions, although the specifications may depend on the specific modality adopted (**Table 1**). The use of patterned light requires precise calibration of light paths and associated bioprinting parameters to enable proper biofabrication of desired volumetric patterns. Such adjustments of light and operational parameters are all very specific to the vat-polymerization modality used, whether it is TPL (used throughout the Primer given its much broader usage than MPL), SLA, DLP, or VAM. It should be clarified that bioprinting by definition is a specific subset of 3D printing, in that the former is described as 3D printing in the

presence of living cells^{1,19}. The same distinction applies when referring to bioink and bioresin *versus* (biomaterial) ink and resin²⁰. For the sake of consistency, we generally employ the terminologies bioresin and bioprinting, although in certain specific descriptions resin and printing may also be used to indicate that cell-laden biofabrication has not yet been demonstrated.

[H2] Bioprinter selection and setup

Vat-polymerization bioprinters can be generally classified by their modes of operations, depending on whether the light for photocrosslinking is projected in a single spot or as a plane, and if the patterning is performed linearly or rotationally. Point-by-point bioprinting relies on laser scanning given the single-spot nature of most laser systems. TPL is a typical bioprinter that utilizes the point-by-point scanning scheme, which builds volumetric structures by raster-scanning the twophoton laser spot across an area and repeating in the vertical direction for each layer to be produced (**Fig. 1a**)^{13,21-23}. A similar operation mode is adopted by the conventional SLA with single-photon laser irradiation (**Fig. 1b**)^{7,24,25}. The raster-scanning approach provides efficient photoreactions due to the larger power densities enabled by the laser lights; however, the inherent larger power densities result in a lower possible cell viability, and raster-scanning is usually a slow process especially when large build volumes are necessary. On the other hand, instead of raster-scanning, a single plane of light can be projected at once to enable simultaneous photocrosslinking of the desired pattern in that layer, followed by layer-by-layer construction leading to the 3D bioprinted structure. A representative modality of layer-by-layer projection-based bioprinting is DLP bioprinting (Fig. 1c)^{11,12,26}. These DLP bioprinters use light-emitting diode (LED) arrays that directly emit patterned light²⁷ via liquid-crystal display (LCD) screens that form digital masks in front of the light source to achieve patterned light²⁸, or digital micromirror array devices (DMDs) that reflect incident light to build patterns²⁹⁻³¹.

Spatial light-modulators like DMDs, are also core technologies in VAM. In this class of approaches, multiple planar light patterns are produced starting from either a laser light or a non-coherent light source and are subsequently projected across the entire volume of the vat^{32,33}. The combination of these projections generates an anisotropic light dose distribution within the vat, so that the cumulative light dose exceeds the polymerization threshold of the bioresin only in correspondence to the geometry of the object to be bioprinted. Currently, VAM is performed either utilizing a single light source projected onto a rotating vat (tomographic bioprinting) (**Fig. 1d**)³²⁻³⁵, multiple light sources delivered onto a static vat (holographic printing)¹⁵, or systems in which a movable light sheet intersects orthogonally with DLP projections to trigger vat-polymerization owing to uniquely designed photoinitiators (light-sheet 3D printing, also known as xolography)¹⁶.

Key considerations regarding the bioprinting modality to select include but are not limited to the resolution, the build volume, the speed, as well as the cost. Laser-enabled vat-polymerization modalities such as TPL, SLA, and VAM that contain high-quality laser systems are generally expensive in particular when multi-photon setups are needed, although resolutions are typically higher than when non-coherent light sources are used (from tens of nanometers for TPL to tens of micrometers for VAM). In comparison, DLP, as well as some VAM and SLA systems that use either non-laser light or low-power lasers, are more cost-efficient despite the reduced resolutions (50-100 μm range). Moreover, as the VAM process addresses the whole volume at once, manufacturing can occur at much high rates (<20 seconds to generate cm³-sized constructs) than most other vat-polymerization strategies¹⁴.

[H2] Software considerations

Software considerations for vat-polymerization bioprinting methods consist of three key components: voxels, which encode the desired input data to be bioprinted; a slicing algorithm, which converts the encoded data to a technique-specific output; and synchronization, which brings together the projection system, motor, and peripherals. As previously stated, vat-polymerization, in its simplest form is the irradiation of light onto a photocurable bioresin; the light takes shape of either a specified point emitted from a laser (in the case of TPL and SLA), or a complete plane of image emitted from a projection device (in the case of DLP and VAM)^{6,36,37}. Therefore, the main objectives are to produce, display, and monitor these images/points in such a way that accurately reproduces the desired model. For the purpose of this section, software considerations will be summarized without taking into account the influences exerted by the bioresin selection, bioresin kinematics, and other bioresin-dependent factors. In addition, for computer-aided design (CAD) software, the reader is referred to the Primer on extrusion bioprinting¹⁸.

[H3] Voxels

Voxels, also referred to as 3D pixels, and their applicability to 3D printing has been explored in great lengths due to their potential to represent 3D volumes, standard tessellation language (STL) files, curves and equations, and point clouds 18,38,39. Voxelization converts input data, commonly STL files, to a conjunction of 3D pixels; a key concept that allows to factor in the limitations presented by the hardware into the software. As an example, if the light source is coming from a DMD device with a resolution of 1920×1080 pixels, then the voxel map typically cannot have more than 1920 and 1080 voxels in the X and Y directions, respectively, unless specialized hardware is employed to allow the movement of the DMD-generated photomask in the XY plane 40. The same principle applies to other light sources (as is the case for TPL, SLA, and VAM) where the resolution of the light is taken as the dimension of the voxel. Voxels can be assigned complex geometries, such as spheres, but for the purpose of vat-polymerization bioprinting it is assumed that an individual voxel is usually given a cubic structure with a unitary value (*i.e.*, high or low) 39. Several open-source software alternatives are available for voxelization in different programming languages, listed in **Table 1**.

[H3] Slicing algorithms

Once the 3D pixel map has been generated (*i.e.*, the input data has been voxelized), the next step is to transform the set of voxels into a technique-specific output by applying a technique-specific slicing algorithm (**Fig. S1**). This is the crucial step that differentiates (from a software perspective) vat-polymerization techniques. As an example, TPL, SLA, and DLP use a slicing algorithm wherein a defined number of voxel layers are grouped along the Z-axis and assigned a weight distribution to produce one image as an output⁶. The number of voxel layers that are grouped together is equivalent to the total number of bioprinted layers. New approaches have been developed to allow freeform bioprinting, where the slice direction is not necessarily parallel to the Z-axis, but rather with variable normal vectors⁴¹. Although other slicing approaches exist for DLP-based techniques⁴², voxelization-to-slicing is a commonly used approach and several open-source software alternatives are available and analyzed in **Table S1**.

In the case of VAM, the slicing algorithm changes according to the specific volumetric fabrication approach selected. In the most common declination of this technology, tomographic bioprinting, the slicing is based on the Radon transform and Ram-Lak filter in the Fourier domain to the voxel map to obtain a set of images which will then be filtered-back projected onto the vat^{32,33}. New tomographic bioprinting slicing approaches to improve resolution have been developed wherein the first step is to apply a correction mask (attenuation correction for example) and from there the same steps are followed⁴³. It is worth mentioning that other technological solutions that belong to the VAM family, such as holographic printing¹⁵ and xolography¹⁶, utilize DLP-like slicing algorithms whose synchronization also differs from tomography-based VAM techniques.

[H3] Synchronization

Once the desired output is obtained, the next step is to ensure the synchronization of all the different components; the most common being the control of a light source and a motor, dictated by the technique employed and the available hardware. For DLP and VAM, since 2D images are projected, the only light source control needed is to specify the duration of exposure and to provide trigger signals⁶. Available software alternatives that facilitate the control of projected 2D images are Psychtoolbox-3 and slmPy for MATLAB and Python, respectively. Other techniques such as SLA have an additional step for the control of the light source; as an example, the tilt angle of a mirror is precisely controlled to direct the laser to specific points⁴⁴. Trigger signals are also needed to specify the duration of light exposure. The light control for these techniques must be synchronized with a motor control, to enable 3D biofabrication. In TPL, SLA, and DLP the motor control is provided by a trigger signal and a specified distance and direction (provided by the desired layer height and selection of bottom-up or top-down approach)⁶. New approaches have been explored to continuously run in parallel light and motor to improve print speed^{45,46}. Other techniques such as tomographic bioprinting have a continuous rotating motor wherein the synchronization is defined by the speed at which the motor rotates and the refresh rate of the projected images^{32,33}. As previously discussed, the synchronization that occurs in xolography¹⁶, though a sub-class of VAM, is more closely related (from a software perspective) to that of continuous liquid interface production (CLIP)⁴⁷ than other volumetric printing methods. Lastly, other peripherals can be added to the bioprinting system, such as sensors and monitoring systems ¹⁶, additional light-sources (dual-color)⁴⁸, as well as a temperature-controlled vat⁴⁹.

[H2] Bioresins

A broad range of synthetic monomer chemistries and functionalized biomacromolecules have been used in vat polymerization-based bioprinting (**Box 1**)⁵⁰. As with other strategies for 3D bioprinting, critical functional requirements must be satisfied by prospective bioresins regarding print stability, cytocompatibility, and bioactivity^{18,51}. However, emerging interests include incorporation of adaptable linkers and/or responsive groups to endow sophisticated 3D structures with more dynamic behaviors (*e.g.*, mechanical transitions relevant to the native cellular microenvironment⁵²) without compromising desired resolution and print speed.

[H3] General considerations on printable materials

Photopolymerization-based bioprinting is amenable to a multitude of bioresins, although complete access to very soft (<1 kPa) biomaterials has been limited by print stability. Specific properties of bioresins depend on processing method. For example, SLA and DLP use low-viscosity bioresins, while TPL/VAM in general requires comparatively more viscous formulations to limit blurring from diffusion of radicals and molecular components, or sedimentation of the as-printed part⁵³. Additionally, bioresin selection has an enormous impact on the pre-polymerization fluid properties, as common high-molecular weight natural polymers are significantly more viscous even at low weight percent (<5%) compared to the relatively low-molecular weight synthetic macromers typically used in vat polymerization. Upon polymerization, user-specified material properties are highly application-, tissue-, and context-dependent⁵⁴, and can be further tailored with light-based crosslinking to construct gradients or other spatial variations in parameters such as stiffness, porosity, and the concentration of network-tethered biomolecules⁵⁵⁻⁵⁸. Moreover, some newer types of bioresins are nano- or micro-composites, incorporating particulate matter within an interstitial matrix^{36,59-61}. These systems have integrated diverse materials, from inorganic or metallic (e.g., silica, graphene, nanohydroxyapatite, gold, strontium carbonate) to polymeric (e.g., chitosan, cellulose, silk, β -lactoglobulin, microgels, emulsion droplets) fillers⁶²⁻⁶⁷. This growing class of composite resins increases functionality for diverse applications in directing cell differentiation, controlling release profiles, or tuning mechanical properties; however, many of these formulations have yet to be applied in vat-photopolymerization bioprinting in particular with the presence of cells. Collectively, these techniques can be used to imbue vat-polymerized biomaterials with nuanced patterning of structure, mechanics, composition, and stimuliresponsiveness.

[H3] Crosslinking chemistry and green strength

215

216

217

218

219

220

221

222

223

224

225

226

227

228

229

230

231

232

233

234

235

236237

238239

240

241

242

243

244

245

246

247

248

249

250

251

252

253

254

255

256

257

258

259

260

Cytocompatibility of the network-forming reaction dictates the success of vat polymerizationbased bioprinting applications. As a result, vat bioresins are typically formulated with poly(ethylene glycol), gelatin, or hyaluronic acid macromers (macromolecular monomers) modified with a variety of reactive groups. For more detailed discussion of specific formulations, we refer the reader to other in-depth reviews regarding photocrosslinkable bioresins 12,22,36,37,54,68. Importantly, the kinetics of the bioresin crosslinking reactions must proceed at an adequate rate to prevent undesirable sedimentation of cells (the latter being a relevant consideration only for techniques in which the resin in a reversible gel state, like gelatin, cannot be used), but also with mild reaction conditions to support cell viability. For photoinitiated polymerizations, some of the mostly commonly used macromers are PEGs, gelatin, and hyaluronic acid functionalized with acryloyls or methacryloyls (chain polymerization) or thiols and norbornenes (step-growth polymerization)⁶⁸. Important distinctions exist between these crosslinking chemistries and strategies for their photoinitiation. Typical bioresin photopolymerizations use 365-nm or visible light (including 405 nm) and water-soluble radical initiators, although specific initiation conditions vary by application and light source. Regardless, the concentration of radicals, cumulative light dose, and incident photon energy must be restricted to a cytocompatible range. Type I photoinitiators (e.g., Irgacure 2959, lithium phenyl-2,4,6-trimethylbenzoylphosphinate (LAP)) undergo homolytic cleavage when irradiated, generating radicals; in contrast, excited type II photoinitiators (e.g., eosin Y, tris(2,2'-bipyridyl)ruthenium (II) chloride) do not fragment but rather produce radicals by hydrogen abstraction or electron transfer with co-initiating molecules⁶⁹, rendering these slower and less efficient due to competing reactions. However, co-initiation by ruthenium and sodium persulfate (Ru/SPS) and visible light has been shown to result in improved cure depths compared to near-UV or visible-light-sensitive Type I initiators⁷⁰.

Chain polymerizations reach the gel point at low conversions (<2%), but are sensitive to oxygen-inhibition, oftentimes require acryloyl-modified biomolecules functionalization, and result in inhomogeneous, brittle networks²². By comparison, the thiol-ene and thiol-yne reactions form more homogenous, tougher networks^{71,72}. These step-growth polymerizations require higher conversion to reach the gel point but are more oxygen-tolerant than chain polymerizations, rendering them very efficient. Moreover, thiol-reactive chemistries simplify network functionalization with biomolecules, as alkenes (e.g., norbornene) readily form thioether bonds with cysteine thiyl radicals. Other bio-orthogonal and initiator-free photoclickable, as well as some photooxidative, chemistries have also been applied to step-growth spatiotemporal hydrogel formation, but these are less common and introduce other challenges relating to synthesis and absorbance⁷³⁻⁷⁵. Recently, photooxidative tyrosine dimerization by Ru/SPS and visible light has been shown to be a highly cytocompatible and capable of crosslinking native tyrosine residues in decellularized extracellular matrix⁷⁶, fibrin⁷⁷, gelatin^{78,79}, and silk^{76,80}, forgoing the need for macromer functionalization. Mixed-mode radical polymerizations (e.g., thiol-acryloyl polymerization) have yet to be implemented in vat polymerization-based bioprinting, but this chemistry provides distinct kinetics, mechanical properties, and degradation profiles as compared to both step- and chain-growth polymerizations⁸¹. Various photochemistries can also be orthogonally and synergistically combined⁸². Next-generation tissue engineering research necessitates facile synthesis and scalability of photopolymerizable bioresins; in this respect, the thiol-ene reaction has been optimized for controlling physicochemical material properties while retaining superior cytocompatibility and kinetics over other radical-induced photopolymerizations^{83,84}.

To further enhance post-polymerization stability, combinations of materials and chemistries have been used to create interpenetrating, dual-crosslinked, or double networks by orthogonal light-triggered reactions⁸⁵ or non-photoinduced, dynamic self-assembly⁸⁶. However, some studies have identified that self-healing, adaptable crosslinks can compromise shape stability in photopolymerized 3D structures, meaning that bioresin formulations containing dynamic bonds should be optimized to balance the benefits of self-healing with long-term print fidelity⁸⁷⁻⁸⁹. Similarly, green strength, or initial post-printing strength, of vat-polymerized biomaterials is important to consider and has been increased in DLP by inclusion of monomers containing ionic or hydrogen bonding sites⁹⁰. Depending on post-printing reactivity (*i.e.*, unreacted functional groups), the final strength of the photopolymerized structures can be improved by flood curing or thermal annealing to induce additional crosslinking⁹¹. However, the initial and final mechanical properties are not always consistently reported and have yet to be compared across various vat photopolymerization techniques. By achieving near-quantitative conversion during the initial photopolymerization, some bioresins (*e.g.*, thiol-ene formulations) avoid post-curing steps, but radical diffusion in such highly efficient systems can limit the resolution of bioprinted features.

[H3] Reactivity, optical properties, and viscosity

261

262

263

264

265

266

267

268

269

270

271

272

273

274

275

276

277

278

279

280

281

282

283

284

285

286

287

288

289

290

291

292

293

294

295

296

297

298

299300

301 302

303

304

305

306

As discussed, many existing photoinitiators have proven effective with cytocompatible light doses used in vat polymerization-based bioprinting. Generally, the concentrations of photoinitiator and absorbers are on the order of millimolar or less with reactive functional group concentrations tens to hundreds of times higher. This suggests that printing increasingly large 3D structures will

mandate more efficiently absorbing initiation strategies and deeply penetrating wavelengths of light due to intrinsic limitations imposed by optical thickness. Near-infrared (NIR)-responsive and upconverting nanoparticles show promise for low-intensity, long-wavelength photoinitiation of common chemistries in bioresin crosslinking^{92,93}, although the cytocompatibility of these methods has yet to be rigorously investigated. Combining photoinitiators with inhibitory molecules has improved feature resolution for some vat polymerization applications, but also slows the overall reaction rate^{22,50}. While rapid reaction rates are desirable to minimize print times, kinetics must be tuned in accordance with light dose and radical diffusion, especially with reactions that are not oxygen inhibited. For example, inclusion of the radical-scavenger 2,2,6,6-tetramethylpiperidin-1-yl)oxyl (TEMPO) was necessary for thiol-ene-based VAM of tubular structures, which otherwise could not be constructed without the TEMPO-mediated inhibition period⁹⁴.

Photoabsorbers, which are usually non-reactive molecules containing chromophores that absorb light in the same range as the initiator, are used in bioresins to reduce light penetration depth, preventing over-curing and improving feature resolution. A broad range of photoabsorbers have been applied in light-based vat-polymerization bioprinting modalities, including Ponceau 4R, tartrazine, curcumin, and anthocyanin, as well as nanohydroxyapatite and gold and melanin nanoparticles^{68,87}. In recent examples, "two-step" absorption has been demonstrated with various mixtures of initiator, scavengers, and quenchers, wherein an intermediate electronic state between a photoinitiator's ground state and excited, radical-forming state is accessed in the one-photon pathway, overcoming restrictions of two-photon absorption in terms of both speed and resolution^{95,96}. Alternatively, some absorbers are susceptible to photodegradation or photobleaching at specific wavelengths, allowing for other combinations of UV and visible light for 3D spatial control over photoinitiation^{45,97}. Absorbers have also been shown to limit light scattering, which has alternatively been corrected for by continuous gradients in light dose^{43,98}. Finally, optical properties have been directly tuned to account for scattering in cell-laden bioresins using refractive index-matching compounds like iodixanol^{34,99}. Of interest, newer developments have further allowed light-based vat-polymerization to occur in a radical (photoinitiator)-free manner, by taking advantage of a caging/photoactivated uncaging process and photoclick reactions 100.

Beyond the biomaterial components, cells are inherently light scattering, and cell sedimentation can lead to inhomogeneities in cell-laden bioprinted structures. Thus, high-molecular weight photopolymerizable precursors or additives such as Percoll (colloidal silica) have been used to alter bioresin viscosity and reduce cell sedimentation^{22,54,101}, and a buoyancy-assisted DLP system was developed to afford continuous-injection liquid interface polymerization and avoid layering artifacts and cell settling during bioprinting¹⁰². Additionally, diffusion of reactive oligomers in liquid bioresins occurs on length scales that are significant compared to feature sizes in DLP, creating conflicts when optimizing viscosity and extent of reaction¹⁰³. In contrast, VAM can be extended to non-diffusive solid-state bioprinting for special bioresins, as with macromers capable of both thermogelation and photopolymerization¹⁰⁴. Naturally, initiator concentration and light dose must be carefully balanced with the chosen bioresin formulation to achieve desired reaction kinetics, all while controlling viscosity and resolution (*e.g.*, *via* inclusion of absorbers or inhibitors).

[H3] Photodegradation and sacrificial materials

TPL has been used to selectively cleave adhesive peptide linkers or degrade channels into premade hydrogels for perfusion or cell guidance using photocleavable moieties, such as nitrobenzyl, among others 105-107. However, the strong absorbance of intrinsically photodegradable functional groups limits the maximum thickness of bioresins incorporating these chemistries, but certain strategies have exploited photoinitiation to induce degradation. For example, allyl sulfides and disulfides have limited intrinsic absorbance, but participate in bond scission cascades amplified by radical propagation, reducing the optical thickness and number of incident photons required for efficient de-gelation 108,109. DLP and other vat polymerization techniques have been utilized to generate degradable hydrogel and elastomer scaffolds to template contractile soft tissue constructs, perfusable vasculature, and topographically defined intestinal stem cell monolayers 110-113. Although photocleavable units have yet to be widely incorporated into bioresins for vat polymerization, other sacrificial (e.g., hydrolytically degradable, enzyme-cleavable, thermoreversible) or phase-separating components can be introduced for production of high-fidelity and intrinsically porous or vascularized 3D biomaterials ^{66,67,114-116}. Ultimately, light-based crosslinking of bioresins makes the fabrication of microscopically complex synthetic 3D tissues possible, with a variety of possible formulations to optimize print fidelity and enable versatile post-printing modifications.

[H2] Variations in vat-polymerization bioprinting techniques

[H3] Bottom-up versus top-down configurations

352

353

354

355

356

357

358

359

360

361

362

363

364

365

366

367

368 369

370371

372373

374

375

376

377

378

379

380

381

382

383

384

385

386

387

388

389

390 391

392393

394

395

396

397

In SLA and DLP bioprinting, since 3D structures are formed eventually through a layer-by-layer method no matter if within each layer, the pattern is created *via* raster-scanning or single exposure, different directions towards the layer-by-layer construction can thus be utilized. The bottom-up configuration pulls the construct up as a preceding layer is crosslinked, exposing the space between the layer and the vat bottom with the liquid bioresin for patterning of the next layer (Fig. 1c). Such a configuration is widely adopted, which confers the ability of 3D bioprinting with minimum bioresin usage and is convenient in most application scenarios. Nevertheless, because a bioprinted structure would need to be pulled upwards and out of the liquid bioresin as the crosslinked thickness increases, it would necessitate sufficient mechanical properties of the bioresin in its crosslinked state to ensure integrity during bioprinting process in combating the gravitational force. This dilemma is effectively addressed by switching the configuration to the top-down setup, in which the build plate is gradually moved downwards as each layer is patterned (Fig. 2a). As such, however, it is easily imagined that the vat must be deep enough to accommodate the entire thickness of the structure to be bioprinted, plus the depth of the build plate itself, leading to significant waste of bioresin. An additional disadvantage of the top-down configuration is the surface tension that may disturb the smoothness of the liquid bioresin between the preceding layer and air to be patterned, causing unwanted reduction in printing fidelity.

[H3] Multi-material bioprinting

The ability to integrate multiple bioresins to introduce heterogeneity into bioprinted constructs is always instrumental to the engineering of structurally and functionally relevant tissues. Unlike nozzle-based or droplet-based bioprinting modalities, the unique requirement of successive operations within a vat for vat-polymerization bioprinting, poses some limitations when one

intends to achieve multi-material fabrication. To date, multi-material vat polymerization has been achieved by several approaches^{6,117,118}. One obvious solution is the use of multiple vats or similar configurations in SLA or DLP bioprinting (**Fig. 2b**)^{119,120}; as a layer of a different bioresin needs to be patterned, the previously bioprinted structure can be moved to another vat filled with the desired bioresin, with a washing process in a separate vat when switching back and forth. Alternatively, a single vat can be used with manual injection and depletion of different bioresins^{30,121}, or adopting a centrifugation approach to aid the removal of the bioresin during switching¹²². This set of methodologies are conceptually and instrumentally simple but is time-consuming due to the numerous steps involved.

To streamline these various steps, alternatively, it has been shown that by introducing a microfluidic chip device into the system design in replacement of the traditional open vat, it is possible to realize automated bioresin-exchange and washing procedures (Fig. 2c)^{123,124}, greatly improving the efficiency of multi-material bioprinting. When a microfluidic chaotic mixer is further adopted either alone 125 or placed in front of the microfluidic chip device 57, on-the-fly modulation of bioresin configurations or continuous gradients would be attainable. A more recent report proved the use of bioresins injected through microfluidic channels dynamically created and integral to a printed construct to realize multi-material DLP fabrication⁴⁶. Despite that these multimaterial abilities are potentially transferrable to TPL or VAM, rare demonstrations have been reported mostly due to the lack of moveable anchors for the photopatterned structures currently available in these modalities. Moreover, oftentimes solid (physically gelled) bioresins are utilized in these two technologies to aid the bioprinting process, which naturally makes more complicated the possibility of multi-material bioprinting, despite that multi-material constructs having spatially separated zones can still be obtained by filling the vat with multiple bioresins in parallel¹²⁶. Of note, one strategy of bioprinting with heterogeneous material properties that might be suitable for all the vat-polymerization methods discussed is that taking advantage of the multi-wavelength bioprinting. This method was originally shown for simple photopatterning¹²⁷ then in DLP printing (Fig. 2d)^{128,129}, where photoinitiators activatable under different wavelengths coupled with different photochemistries allowed crosslinking of specific components in a multi-component bioresin vat, and was recently adapted for tomographic printing as well⁴⁸. Similarly, grayscale fabrication using intensity-gradient photomasks is able to generate printed structures with mechanical property heterogeneities 130,131.

[H3] Converged approaches

Each bioprinting technique has its own limitations, and thus there is a trend in the field of biofabrication to merge technologies and gain the advantages of two or more bioprinting modalities. For example, a DLP printer has been combined with an extrusion-based printer towards engineering interface tissues bearing unique property requirements for different segments ¹³². DLP can also be integrated with e-jet printing to produce hybrid electronic devices ¹³³, or acoustic-assisted printing to achieve necessary alignments across the layers ¹³⁴⁻¹³⁶. Within vatpolymerization bioprinting, both DLP ¹³⁷ and tomographic printing ¹³⁸ have been separately combined with TPL to enable 3D printing of constructs with feature resolutions across multiple scales, and tomographic printing has also been combined with melt electrowriting, to build fiber-reinforced structures ¹³⁹.

[H1] Results

Light-based vat-polymerization bioprinting technologies enable the use of intricate designs for a rapid generation of complex bioprinted structures. Still, the generation of high-resolution structures with enhanced functionality, stability, and mechanical properties requires optimization of used bioresins and different printing parameters such as light dose, print speed, or layer thickness depending on the used bioprinting technique. Even after successful bioprinting, freshly fabricated cell-loaded constructs have to mature into biologically functioning tissue equivalents. This requires material stability, biocompatibility, and delivery of appropriate cell-material interactions guiding tissue morphogenesis, as well as specialized post-processing, culture, and preservation conditions. Accordingly, the methods to assess printability parameters, resolutions, and biological functioning and maturation of the bioprinted constructs are discussed.

[H2] Printability assessment

[H3] Light-dose response and working curve generation

In all light-based vat-polymerization techniques, the printability and resolution are intimately dependent on the kinetics of the photocrosslinking reaction, and therefore unique for each bioresin formulation⁸⁷. A key parameter to be optimized and enabling printability is the amount of light energy (dose) that is supplied to each voxel. Too low doses lead to insufficient crosslinking and failure to develop the smallest feature sizes, while too high doses can lead to over-crosslinking, and loss of resolution due to off-target polymerization ^{114,140}. In the context of SLA/DLP, therefore, a first step is to assess the relation between different irradiation conditions and the spatial propagation of the polymer crosslinking within the bioresin vat, a relation estimated by the working curve for the given photopolymer. A simple method to establish the SLA/DLP working curves consists of projecting onto the bioresin vat an array of spaced disks or squares, with each sample exposed to an increasing light dose (Fig. 3a). The irradiation pattern can also be randomized to minimize the effect of possible unequal illumination across the build window¹⁴¹. For higher light doses, light will travel further into the bioresin (curing depth, C_d), causing the crosslinking of a thicker structure. After irradiation the uncured bioresin is washed off. Depending on the stiffness of the resulting hydrogel constructs, and on how close to each other these have been crosslinked, their thickness can be measured with a caliper, a profilometer, a micrometer, or from microscopy images, and then recorded to create a light energy versus thickness plot (Fig. **3b**). The working curve is then defined by the following equation, where D_p indicates the light penetration depth, and E_c the minimum energy needed to crosslink the photopolymer:

$$C_d = D_p \cdot ln \frac{E}{E_C}$$

This information is crucial to select the photoexposure condition and the layer height that can be targeted when bioprinting (and therefore the highest resolution achievable in the z-direction, or axial resolution). However, it should be kept in mind that, in practice, the light intensity is not perfectly uniform throughout the thickness of the layer 142. The light intensity tends to drop off as it moves through the bioresin due to absorption effects, and therefore the layer starts crosslinking closer to the light source and grows in thickness over time during the photoexposure step, until it reaches the previously crosslinked layer. Therefore, to ensure effective binding of a layer onto the previous one, exposure time should be slightly increased above what is identified according to the

working curve. The exact light dose (and layer height) can be fine-tuned empirically with test prints.

In tomographic bioprinting, identification of the workable light dose range is the first step towards printability. As this approach is layer-free, and in principle all the parts of the object are crosslinked at once and near-simultaneously, a key parameter governing printability is the threshold energy needed to initiate photocrosslinking, which can also be detected with a dose test, similar to those classically used in TPL optimization¹⁴³. Typically, an array of disk-shaped spots is projected across the build volume, in which a static, non-rotating square cuvette containing the bioresin is placed (**Fig. 3c**). Each spot corresponds to a given light intensity and exposure time (usually varying from a few seconds to no more than a couple minutes). In tomographic bioprinting, different from SLA and DLP, light needs to travel all the way through the vat in the direction longitudinal to the projections, with at least 37% of the incoming light intensity reaching the opposite edge of the vat¹⁴². Thus, rather than measuring the C_d, the lowest dose required to obtain a crosslinked disk that bridges the entire thickness of the cuvette is recorded as needed to ensure printability⁸³.

[H3] Resolution assessment

488

489

490

491

492

493

494

495

496

497

498

500

501

502503

504 505

506

507

508

509

510

511

512

513

514

515

516

517

518

519

520

521

522

523

524

525

526

527

528

529

530

531

532

Resolution in light-based vat-polymerization directly correlates with the capacity of the bioprinting process to confine the photocrosslinking reaction within the desired voxel, and therefore is correlated to the optical voxel size (e.g., size of the laser spot or of the pixels on the DMD), the light dose distribution inside and outside the voxel of interest, and the mobility and diffusion of the reactive species triggering the crosslinking¹¹². Resolution also differs depending on the axis along which it is measured in the produced object (i.e., longitudinal or orthogonal to the direction of projection of the light), and if the measurement refers to positive features (e.g., spikes, tips, pillars) or negative features (e.g., channels, pores, voids)¹⁴⁴. Typical assays to assess resolution in layer-by-layer vat-polymerization consist of printing diagnostic models with small positive features, such as rectangular posts ranging in size at light-exposure parameters in the optimal range identified with the working curve. At decreasing exposure, the smaller positive features are not formed and with half the light energy only the largest ones will form but they will be weaker and thinner than they should be. However, simply maximizing exposure leads to overprinting ¹⁴⁵. This is especially relevant for printing negative features: when printing gaps of different size, highexposure printing will resolve the larger gaps but will lead to complete fill-in of the smaller ones effectively lowering the resolution (Fig. 4a). More notably, in point-by-point and layer-by-layer methods the axial resolution, longitudinal to the light projection, is determined by the layer thickness. Overcuring utilizing too high light doses can therefore lead to difficulties in printing overhangs and pores oriented along the XY plane, since if the C_d is longer than the layer height, pores in adjacent layers will be clogged by partly crosslinked bioresins. All these effects can be quantified by printing at different layer thickness test models, such as cubes with longitudinal pores (of cylindrical or squared section) of different sizes 146. Finally, since each layer is composed by joined rectangular voxels, the surface of the printed objects can display a pixelated profile, which can be readily evaluated through microscopy images, depending on the resolution of the device¹⁴⁷. For the same region, cross-sections of the object to be printed can also reveal a clear layering pattern that depends on the layer thickness (Fig. 4b). While this printing artefact could also be exploited to introduce roughness useful for aligning cultured cells via contact guidance,

continuous bioprinting approaches, such as CLIP and xolography can be used to minimize their appearance¹⁴⁸.

In tomographic bioprinting, the planar axis, which is perpendicular to the light direction, and the tomographic axis, which is parallel to the direction of light, have different phenomena that are governing their resolution. The surface of the DMD is imaged into the vial containing the material. The voxel resolution in the center of the build volume is determined by the pixel size of the modulator and the magnification of the lens system. However, at a distance from the center of the printed object the effective pixel size increases proportionally to the divergence of the illumination beam. The etendue of the illumination source and the accuracy of the volumetric dose reconstruction leads to decrease in resolution, which can be limited by using illumination source with a low etendue¹⁴⁹. In addition, overall resolution might be affected by the diffusion of radical species and sedimentation of the printed object¹⁵⁰. Use of the bioresins with high viscosities (>10 Pa s) counteracts the sedimentation of the printed object below 10 μm¹⁴⁹, an effect that can be even negated by the use thermoreversible gelling materials such as gelatin. Moreover, highly viscous resins also limit the diffusion of the radical species outside of the voxels of interest³³. Resolution assessment is performed by printing the object with positive and negative features (Fig. 4c), which can then be analyzed with microscopy³⁴. To facilitate visualization of small negative features and improve their imaging contrast, the hydrogel bioresin can be formulated with a fluorescent dye or oppositely the hollow object can be filled, for instance, with fluorescent dye (Fig. 4d).

[H3] Metrology, image-reconstruction, and imaging techniques for characterizations

An initial printability assessment during the printing process is done using a monitoring camera. After the sample is printed it can be inspected visually and using simple stereomicroscopy. For a more precise analysis microcomputed tomography (μ CT) can be performed to reproduce full sample architecture. Alternatively, printed objects can be scanned in 3D with resolutions down to 0.01 mm or imaged using a lightsheet microscope, confocal microscope or a fluorescent microscope equipped with computation clearing. The imaged 3D object can be reconstructed using microscope specific software such as LAS X (Leica) or ZEN (Zeiss) or open-source software like ImageJ or nRecon and after correction of light distortion in the z-dimension the image can be reconstructed in 3D. For specific analysis, the reconstructed sample morphology can be compared to the original 3D model of the object using ImageJ plugins or specified software such as Cloudcompare. These software tools compare the STL file of the model to that of the bioprinted sample and calculate the differences of the volume fidelity between them giving the sample-to-model fidelity in percentage. For example, volumetric bioprinting shows on average volume variation of below 5-10% when comparing the printed constructs acquired via μ CT and the original STL files³³.

[H3] Cellular assessment

The bioprinted constructs can be stored, cultured, and analyzed similarly to cell-laden photocurable hydrogels, which are frequently used as 3D culture systems¹⁵¹. In contrast to extrusion-based bioprinting¹⁸, light-based vat-polymerization bioprinting techniques are nozzle-free, and do not impose high shearing forces on the encapsulated cells avoiding destruction of cluster architectures, organizations, and cell-cell interactions³⁴. Typically, the use of light-based polymerization, especially in the UV-A and near-UV visible-light range, together with free-radical

generation common to many photochemistries used in vat polymerization, may rise concerns regarding potential cell impairment, and therefore assessments evaluating the presence of absence of DNA damage or oxidative stress can be beneficial¹⁵². It should also be noted that previous literature has extensively reported safe photoexposure windows of parameters in which no lasting cell impairment is found even with proteome analyses¹⁵³, and that photoreactive hydrogels can protect the cells from free radicals, as the radicals are captured to trigger crosslinking reactions, such as in chain-growth polymerization¹⁵⁴. Additionally, the maturation capacity of the encapsulated cells demonstrates compatibility of bioresins, bioprinting process, and subsequent culture conditions, which takes place over several days to weeks, in some cases even months. In the case of organoids or stem cell clusters, maturation is demonstrated by the ability of the encapsulated cells to differentiate and to form highly organized structures resembling the natural architecture of the target organs¹⁵⁵. Advanced maturation is associated with obtaining organ-specific functionality, *e.g.*, measuring the electrophysiology in stem cell-derived neuronal cells¹¹³, and ability of ammonium-elimination from perfusate for liver organoids³⁴.

[H1] Applications

Light-based vat-polymerization bioprinting represents a promising technology for a wide range of biomedical applications. This section offers an overview of the various strategies exploited for engineering structurally and physiologically relevant tissues towards regenerative medicine and tissue models for use in drug discovery.

[H2] Point-by-point scanning

Two-photon irradiation can be exploited in multiple ways, from polymerizing 3D scaffolds^{22,156-159} and patterning them with bioactive molecules^{55,160-163}, to degrading them by means of photocleavage reactions^{106,164,165} or ablation (**Fig. 5a**)^{138,166,167}. However, due to the limited build volume and long printing process, TPL has been so far largely limited to constructs ranging from hundreds of micrometers to few millimetres^{22,156}. This limits the ability of TPL to target tissue- or organ-size, but it holds great promises for high-precision bioprinting of microtissue models^{138,157,158,165,168,169,100,170-172}, production of soft microstructured cell/drug delivery systems (*i.e.*, microneedle arrays or microrobots)¹⁷³⁻¹⁷⁷, and the study of cell mechanobiology^{178,179}. Moreover, thanks to the intrinsic confocality of two-photon irradiation and enhanced tissue penetration of NIR wavelengths, TPL has also been explored for printing *in vivo*¹⁸⁰, and inside (synthetic) cells¹⁸¹.

[H2] Layer-by-layer projection

Projection-based lithography has been used with a variety of cell types, such as stem cells and their derivative cell types 30,58,113,182 , mesenchymal stem cells $(MSCs)^{57,183}$, adipose-derived stem cells 184,185 , endothelial cells 57,58,183,186,187 , myoblasts 57,188 , hepatic cells $^{189-191}$, chondrocytes 192 , and tumor cells 193 , showing good biocompatibility (cell viability $\geq 70-80\%$), thus opening the way to various tissue targets.

Of pivotal importance for the successful engineering of large tissue constructs, DLP has gained particular interest for the generation of multiscale vasculature networks^{114,194,195}. This has been elegantly demonstrated by the generation of 3D entangled vascular networks resembling alveolar

topology (**Fig. 5b-i**)¹⁴⁶. *In vitro* and *in vivo* studies confirmed the potential of this method to generate large, vascularized tissues for regenerative medicine. This technology, acquired by 3D Systems, has progressed toward full size lung constructs with micron-level capillaries and is heading toward pre-clinical transplantation studies in collaboration with Lung Biotechnology PBC (United Therapeutics)¹⁹⁶. Also recently, the high-fluidity-photoresin approach was leveraged to bioprint large, clinically-relevant-sized cell-laden hydrogels featuring vessel networks (**Fig. 5b-ii**), thus maintaining high cell viability in the core of the construct thanks to improved nutrient and oxygen transport¹⁹⁷.

Besides vascularized constructs, DLP holds great promises for the printing of a wide variety of other cell-laden implants and tissue models. For example, it has been used to bioprint cartilage^{184,192,198}, bone¹⁹⁹, corneal¹⁸⁵, glioblastoma²⁰⁰, and liver^{201,202}-like tissues as well as acellular heart valves²⁰³, bone implants^{204,205}, vascular grafts²⁰⁶, and nerve conduits²⁰⁷⁻²⁰⁹. Another DLP-enabled technology termed filamented light (FLight) biofabrication has also recently emerged as a promising method to bioprint aligned tissue constructs with unprecedented speed and cell guidance capabilities (**Fig. 5b-iii**)²¹⁰. In addition, DLP has been explored for non-invasive, *in vivo* bioprinting. In contrast to the conventionally used 365–405-nm irradiation, the higher tissue penetration capacity of near-infrared light (980 nm) was exploited to photocrosslink 3D structures *in situ* within subcutaneously injected photoresin²¹¹. Interestingly, DLP can be exploited to manufacture programmable shape-morphing hydrogel constructs (four-dimensional (4D) printing), thus making it possible to obtain complex 3D geometries and curvatures from relatively simple prints^{212,213}.

Extracellular matrix (ECM) and cellular heterogeneity strongly contribute to the mechanical and physiological functions of human tissues. Using a nitrobenzyl-modified chondroitin sulfate to mitigate excess of free radicals diffusion, high-resolution, multicellular bioprinting of liver units was reported¹⁹¹. In other examples, geometric complexity was combined with regionally varied stiffness^{189,214} or with post-printing patterning of bioactive molecules⁵⁸, thus further improving the functionality of the biomimetic cell microenvironment. Cell spreading and nutrient exchange can be modulated and improved with the use of bioresins containing porogens, which is of particular importance for large tissue constructs^{57,66,67,114,116}.

Overall, projection-based bioprinting offers an unprecedented opportunity to biofabricate large, yet highly complex tissue architectures. However, to date high resolution has been generally achieved with highly concentrated photoresins (typically >10% GelMA or PEGDA), thus resulting in stiff constructs. Recently, a post-printing molecular cleavage approach was proposed to tune the mechanical properties of the bioprinted constructs without affecting their structural complexity 113, opening new avenues for DLP-based bioprinting of ultrasoft tissues (**Fig. 5b-iv**).

[H2] Volumetric approaches

Despite being in its infancy, tomographic printing has been already explored to generate vascular-like constructs^{80,149,215}, as well as bioprinting of cartilage-³³, muscle-⁸³, liver-³⁴, and bone-like²¹⁵ tissues (**Fig. 5c**). The rapid fabrication times and the absence of mechanical stresses imposed to cells, can be particularly beneficial for applications in which fragile cellular structures (i.e. epithelial organoids) are involved³⁴. Contrary to SLA and DLP, tomographic bioprinting requires high photoresin transparency for the light to penetrate through the whole printing volume. This aspect intrinsically limits the number of suitable photoresins, as well as the density of embedded cells (typically <2×10⁷ cells mL⁻¹), if strategies that mitigate light scattering caused by intracellular

organelles are not in place. In particular, low cell densities are less desirable as the biofabrication field moves towards increasingly high-cell-density bioinks and bioresins (tens/hundreds of million cells mL⁻¹)²¹⁶. With current capabilities, tomographic bioprinting is a manufacturing method better indicated to generate relatively low cell densities, centimeter-scale tissue constructs, free-form soft robotics components and perfusable tissue models for organ-on-chip technology. Significant advances for tomographic bioprinting competitiveness could result from the introduction of multimaterial/multicellular printing strategies¹²⁶, elimination or enabling to design self-focusing-induced microporosity^{138,217}, and further improvement of positive and negative resolutions which are to date generally equal or lower to SLA and DLP.

[H1] Reproducibility and data deposition

Several factors can influence the reproducibility of vat-polymerization bioprinting processes and the quality of resulting bioprinted tissue constructs. To ensure extended applications of these bioprinting techniques, considerations in multitude of parameters such as bioink designs and preparations, operational procedures, as well as data reporting and repositories shall be carefully taken.

[H2] Bioresin considerations

Since photoactivatable bioresins are key to any of the light-based vat-polymerization bioprinting techniques, the biomaterials oftentimes would need to be functionalized from their pristine forms to be usable. Synthetic biomaterials are usually more reproducible especially those that can be commercially sourced that have undergone proper quality controls. Naturally derived biomaterials, on the other hand, can be quite inconsistent in their reproducibility due to multiple reasons. One is the nature of these biomaterials; since they are produced from natural tissues, depending on the species and tissue type they are coming from, as well as their processing method, the raw, unmodified biomaterials are already inconsistent in their properties made up of molecules of varying molecular weights and molecular sequences or configurations, in particular with protein-based biomaterials. Then, with further functionalization to endow these biomaterials with photoactivatable moieties which involves additional processing steps, more variabilities may be introduced leading to quality concerns for these naturally derived biomaterials when they are used as bioresins for bioprinting.

Some new developments have shown the potential to simplify the problem, to some degree. For example, the relatively recently reported photoinitiator of tris(2,2-bipyridyl)dichlororuthenium(II) hexahydrate (Ru)/sodium persulfate (SPS)^{77,78}, enables efficient formation of crosslinks through oxidizing aromatic residues such as those in tyrosine leading to generation di-tyrosine bonds with adjacent tyrosine groups. Accordingly, protein biomaterials in their unmodified form can be directly photocrosslinked as long as sufficient tyrosine groups are present on their molecular chains, such as fibrin⁷⁷, gelatin⁷⁹, decellularized ECM (dECM)⁷⁶, and silk^{78,80}, among others.

Incorporation of cells poses another major factor contributing to reproducibility issues. Beyond the cell-source variability that is universal to any biofabrication methods, the cell type and density also matter in terms of determining bioresin performances due to the light-based production procedures that are easily impacted by scattering and diffraction of incident light. A recent publication indicated that by introducing cytocompatible refractive index-matching compounds

such as iodixanol, VAM³⁴ or DLP⁹⁹ bioprinting in the presence of high cell densities is possible without significantly sacrificing the resolution. Another concern is the sedimentation of the cells during the bioprinting process, which can be addressed in TPL and VAM using physically gelled solid bioresins, which nonetheless, remains as a major obstacle for SLA and DLP bioprinting as liquid bioresins would have to be used in these setups.

[H2] Other operational considerations

Although the effect of bioresin viscosity is not as strong as in some other bioprinting methods such as extrusion (high viscosity values) and inkjet (low viscosity values), it is also a factor to consider in vat-polymerization techniques. TPL when it comes to photocrosslinking as well as VAM, as discussed above, can accommodate wider ranges of bioresins since both liquid and solid bioresins can be used towards fabrication as long as the structures are anchored to the surface of the build plate. For photodegradation TPL, in contrast, it has to start with solid bioresins given the fact that the patterned freeform hollow structures need to be mechanically supported to avoid shape change. For SLA and DLP bioprinting, the bioresins need to be in the liquid form, however a wide range of bioresin viscosities can be used (10–5,000 mPa·s). It is important to note that parameters such as ambient temperature could affect the reproducibility especially for temperature-sensitive bioresins such as those based on gelatin. To this end, the utility of fish gelatin and its derivatives shows advantages due to their lower responsiveness to temperature compared to porcine counterparts¹¹⁴.

Bioprinter hardware and software further contribute to the reproducibility performance of vatpolymerization platforms. Examples include control precision such as that for motor movements in the x-y plane (for raster-scanning mode), the z direction (for both point-by-point and layer-bylayer scanning modes), and the rotation (for tomographic printing). However, unless the systems are custom-built, the freedom of such controls are always limited when commercial bioprinters are used. Unlike extrusion bioprinting, path planning may not aid much in vat-polymerization bioprinting.

[H2] Reporting and data repositories

Not only the bioresin and procedure standardizations are lacking for vat-polymerization bioprinting, but also the standardization in reporting is rarely considered by the community. In **Box 2**, we list a collection of key reporting items that are instrumental to ensuring sufficient information is included in an any given publication for others to be able to effectively reproduce the results. Similarly, the databases for vat-polymerization bioprinting, or bioprinting in general, are scarce. The <u>3D Printing Database</u> is one such database dedicated to 3D printing and bioprinting collectively, yet the number of parameter items is still very limited and does not classify by printing or bioprinting modalities, which require distinct sets of reporting parameters for their operations (see those necessary for extrusion bioprinting¹⁸). An additional database is <u>GitHub</u>, a repository of software and firmware version-control and collaboration platform including those for vat-polymerization bioprinting. In general, a trend is that databases for open scientific and research data-sharing are becoming increasing more common, with examples being <u>Zenodo</u> and <u>Mendeley Data</u>, among others.

[H1] Limitations and optimizations

Different vat-polymerization bioprinting techniques have their own unique advantages and disadvantages, resulting in the different ranges of key performance indicators that each of them can achieve towards various applications in tissue fabrication (**Table 1**). In this section, some major limitations of these vat-polymerization bioprinting techniques are discussed with potential solutions to optimizations also suggested.

[H2] Combating the mechanical property-gravity balance in SLA/DLP bioprinting

As we discussed previously, SLA and DLP bioprinting can be divided into top-down and bottom-up configurations. Although the former is not significantly influenced by gravitational force during the 3D construction process since the platform is always immersed within the liquid bioresin, it is plagued by surface tension problems as well as the significant waste of the bioresin. On the other hand, the bottom-up approach uses the minimal bioresin possible, but since the upward-pulled parts often are exposed to air out of the liquid bath, it is difficult to maintain integrity of the bioprinted structures in particular when soft tissues need to be engineered. Several methodologies have been proposed accordingly. In one example, a fluid support was utilized to introduce buoyancy force in mitigating that caused by gravity, during the pulling steps¹⁰². Alternatively, the bioresins can be meticulously designed, such as using a multi-component bioresin of GelMA and HAMA, which enables stiff constructs to be created initially while the HAMA molecules are subsequently selectively cleaved to return the mechanical properties back to those controlled by the low-concentration GelMA¹¹³.

[H2] Addressing limitations of reconstruction in tomographic bioprinting

Of all the techniques belonging to the family of vat-polymerization, tomographic bioprinting is one of the most recent to date, and, albeit promising, it is still in its infancy. Further research efforts are required to advance this technique. In terms of software and reconstruction algorithms, the current versions are directly derived from processes commonly utilized in tomographic imaging, where the filtering and back-projection steps produce a virtual image, rather than a physical object. The Ram-Lab filter returns projections with both negative and positive values, the former of which would require sending light capable of inhibiting the crosslinking reaction. While this concept has been already demonstrated²¹⁸, the practical implementation is not trivial, and current algorithms circumvent this challenge by thresholding and setting the negative values to zero. As this results in the accumulation of high undesired light doses in certain off-target regions of the design, in some cases it could partly overcure thin features, therefore reducing the achievable resolution. While algorithms including corrections to improve contrast between on- and off-target regions of the vat are being successfully developed 149,219, further research in printing-dedicated tomographic reconstructions is needed to maximize the resolution of tomographic bioprinting. This is also especially relevant for the field of bioprinting, where the accuracy of the tomographic printing process can be hampered by light scattering caused by cells, microparticles, and ECM aggregates. Methods to adjust the refractive index of the bioresins with biocompatible index-matching compounds, and to computationally minimize the effect of scattering via optimizing the filtered tomographic back projections have already been successfully implemented^{34,43}.

[H2] Improving the speed and resolution of vat-polymerization bioprinting

The various vat-polymerization techniques feature different bioprinting speeds, with tomographic bioprinting being the fastest since the time needed for production does not necessarily scale with the volume, while in DLP the speed is linearly related to the thickness of the construct and for SLA and TPL the speed scales with the volume. Despite these differences, there are generally methods to improve the bioprinting speed of each modality. In DLP for example, by building an oxygen-containing "dead zone" into the bottom of the vat separating the patterned layers with the vat surface, the continuous liquid interface approach enables fast creation of volumetric structures 47,146,197,220. The speed of DLP process may be further enhanced by embedding a bioresin-immiscible fluid layer as the "dead layer", which is further circulated to dissipate heat generated from photopolymerization 221. For SLA, the speed is aided by the light-sheet system 222. A multi-focus process that simultaneously generates and controls up to ten laser foci further enables parallel nanofabrication through TPL 223; alternatively, multiple beams can be used to also expedite the TPL procedure 224.

In terms of resolution, the performance is in the reverse order of the operational speed for the modalities, *i.e.*, TPL gives the highest resolutions (tens of nanometer-range) followed by SLA, DLP, and VAM bioprinting techniques (micrometers to tens of micrometers) and resolution scales can vary depending on the specific setups. Some broad strategies for resolution-enhancement include the utilization of 8K/16K DMD or other projection systems as the light-pattern sources. Other interesting methodologies can further increase the fabrication resolutions without hardware upgrade. These methods include the synergy of two light sources, one photopolymerizes and the other inhibits polymerization⁴⁵; volume shrinkage post-bioprinting²²⁵⁻²²⁷; as well as the integration of feedback and correction algorithms into the software^{149,228}.

[H1] Outlook

In the last decade, light-based vat-polymerization bioprinting has gained traction within the fields of bioprinting and tissue engineering. The adoption of light-based vat-polymerization bioprinting is evidenced in multiple commercial systems recently coming to market⁵. There are several exciting emerging use cases as well as technological developments that, if validated, will enhance the performance and scope of light-based vat-polymerization bioprinting as both a powerful tool for life science research and clinical applications.

First, we are excited about early work in intelligent bioprinting by integrating machine-learning with light-based bioprinting. One of the limiting factors of the spatial resolution of light-based polymerization, which is only exacerbated in cell-laden bioprinting, is the effect of light scattering²²⁹. The effect of light scattering on resolution can be reduced to an extent by trial-and-error modification of the printing parameters and printing solution composition (*e.g.*, by adding photoabsorbers); however, this is a tedious, time-intensive process and likely not to result in optimal resolution for fine features. Recently, machine-learning using deep neural networks has been shown to be capable of generating digital masks with a modified geometry and grayscale values to produce a 3D-printed part of a preset specification with superior microscale resolution as compared to trial-and-error optimization^{230,231}. Going forward, continued development in machine learning optimization of key properties of a bioprinted device or tissue such as the resolution and mechanical properties, will eventually enable one to specify desired properties of a bioprinted construct for any given arbitrary geometry and known printing solution composition. A recent report showed a contrast-based focusing mechanism that could be automated for consistent

single-digit microscale²³². Automated focusing coupled with machine-learning optimization will eventually enable a lay user to simply input their 3D image file and desired mechanical properties and the bioprinting system will do the rest.

Further, there are currently no bioprinting solutions used in the clinic as the commercial use of the technology is in the nascent stage. The United States Food and Drug Administration (FDA) has only just begun in the last year to consider developing regulatory guidance on using 3D printing technology in the clinical setting²³³. Light-based 3D printing is already widely adopted by the dentistry field, where practitioners use 3D scanners with 3D printers to fabricate a myriad of patient-specific solutions ranging from crowns to surgical implants to mouthguards and retainers^{234,235}. The FDA has not produced guidance on combining human cells or tissue with 3Dprinted constructs in the clinic, let alone bioprinting. Light-based bioprinting has the greatest potential of the bioprinting modalities to be incorporated in the clinical setting as it has the quickest production process, does not induce mechanical stress on the cells, and is capable of providing the highest resolution. Due to the complexity in optimization and need for consistent microscale resolution to match injury-specific build specifications, automating the bioprinting process will be a necessary leap to integrate it into the clinical setting. Additionally, clinicians will need to be able to readily develop a bioprinted scaffold therapy based on a patient's defect upon presentation. Already researchers have shown that they can transform 3D medical images into structures that match the geometric shape of a defect site²⁰⁹. To achieve bioprinting at the point-of-care, a turnkey ecosystem will have to be developed for a clinician to fabricate a patient-specific bioprinted scaffold directly from a 3D medical image of a defect site. Alternatively, intravital bioprinting, i.e., bioprinting directly at the site of injury or defect, has been reported using light-based vatpolymerization techniques ^{180,211}.

Author contributions

Introduction (R.L., O.D., Y.S.Z.), Experimentation (R.L., O.D., C.E.G.-M., B.E.K., K.S.A., Y.S.Z.), Results (R.L., O.D., Y.S.Z.), Applications (R.R., M.Z.-W., Y.S.Z.), Reproducibility and data deposition (R.L., O.D., C.E.G.-M., Y.S.Z.), Limitations and optimizations (Y.S.Z., R.L.), Outlook (J.S., S.C., Y.S.Z.). Overview of the Primer (R.L., Y.S.Z.). Reviewing and editing (all authors).

Competing interests

YSZ consults for Allevi by 3D Systems, and sits on the scientific advisory board and holds options of Xellar, both of which however, did not participate in or bias the work. The other authors declare no interests.

Acknowledgements

R.L. acknowledges funding from the European Research Council (ERC) and from the FET-OPEN scheme under the European Union's Horizon 2020 research and innovation programme (grant agreements No. 949806 and 964497), and from the Netherlands Organization for Scientific Research (024.004.013 and NWA.1228.192.105). B.E.K. and K.S.A. acknowledge funding from the National Institutes of Health (R01DE16523, R01DK120921). J.S. acknowledges funding support from the National Institutes of Health (F31NS125986). S.C. acknowledges funding from

the National Institutes of Health (R01CA253615, R33HD090662, R21ES034455) and the National 901 Science Foundation (1907434, 2135720). M.Z.-W. acknowledges funding from Innosuisse 902 (55019.1 IP-ENG). Y.S.Z. acknowledges funding from the National Institutes of Health 903 (R21EB025270, R01EB028143, R01HL165176, R01HL166522), the National Science 904 Foundation (1936105), and the Brigham Research Institute. 905

Peer review information

Nature Reviews Methods Primers thanks [Referee#1 name], [Referee#2 name] and the other, anonymous, reviewer(s) for their contribution to the peer review of this work.

References

906

907

908

909 910

911

912

913

914

915

- Groll, J. et al. Biofabrication: reappraising the definition of an evolving field. Biofabrication 8, 013001, doi:10.1088/1758-5090/8/1/013001 (2016).
- Levato, R. et al. From shape to function: the next step in bioprinting. Adv. Mater. 32, 2 1906423 (2020).
- 3 Moroni, L. et al. Biofabrication: A Guide to Technology and Terminology. Trends 916 Biotechnol. 36, 384-402, doi:https://doi.org/10.1016/j.tibtech.2017.10.015 (2018). 917
- Moroni, L. et al. Biofabrication strategies for 3D in vitro models and regenerative medicine. 918 4 *Nature Reviews Materials* **3**, 21-37, doi:10.1038/s41578-018-0006-y (2018). 919
- 5 Heinrich, M. A. et al. 3D Bioprinting: from Benches to Translational Applications. Small 920 15, 1805510, doi:10.1002/sml1.201805510 (2019).
- Garciamendez-Mijares, C. E., Agrawal, P., García Martínez, G., Cervantes Juarez, E. & 6 922 Zhang, Y. S. State-of-art affordable bioprinters: A guide for the DiY community. Appplied 923 Physics Reviews 8, 031312 (2021). 924
- (Google Patents, 1986). 7 Hull, C. W.
- 8 Lu, Y. & Chen, S. C. Micro and nano-fabrication of biodegradable polymers for drug 926 delivery. Adv. Drug Del. Rev. **56**, 1621-1633, 927 doi:https://doi.org/10.1016/j.addr.2004.05.002 (2004). 928
- 9 Mapili, G., Lu, Y., Chen, S. & Roy, K. Laser-layered microfabrication of spatially 929 patterned functionalized tissue-engineering scaffolds. Journal of Biomedical Materials 930 Research Part B: Applied Biomaterials: An Official Journal of The Society for 931 Biomaterials, The Japanese Society for Biomaterials, and The Australian Society for 932 *Biomaterials and the Korean Society for Biomaterials* **75**, 414-424 (2005).
- Dhariwala, B., Hunt, E. & Boland, T. Rapid prototyping of tissue-engineering constructs, 10 934 using photopolymerizable hydrogels and stereolithography. Tissue Eng. 10, 1316-1322 935 (2004).936
- Li, W. et al. Stereolithography Apparatus and Digital Light Processing-based 3D 11 937 Bioprinting for Tissue Fabrication. iScience 26, 106039 (2023). 938
- Yu, C. et al. Photopolymerizable Biomaterials and Light-Based 3D Printing Strategies for 12 939 Biomedical Applications. Rev. 120, 10695-10743, Chem. 940 doi:10.1021/acs.chemrev.9b00810 (2020). 941
- Zuev, D. M., Nguyen, A. K., Putlyaev, V. I. & Narayan, R. J. 3D printing and bioprinting 13 942 using multiphoton lithography. *Bioprinting* **20**, e00090 (2020). 943

- Zandrini, T., Florczak, S., Levato, R. & Ovsianikov, A. Breaking the resolution limits of 3D bioprinting: future opportunities and present challenges. *Trends Biotechnol.*, doi:https://doi.org/10.1016/j.tibtech.2022.10.009 (2022).
- Shusteff, M. *et al.* One-step volumetric additive manufacturing of complex polymer structures. *Science Advances* **3**, eaao5496, doi:10.1126/sciadv.aao5496 (2017).
- Regehly, M. *et al.* Xolography for linear volumetric 3D printing. *Nature* **588**, 620-624 (2020).
- 17 Ruskowitz, E. R. & DeForest, C. A. Photoresponsive biomaterials for targeted drug 951 culture. delivery and 4D cell Nature Reviews Materials 3. 17087. 952 doi:10.1038/natrevmats.2017.87 (2018). 953
- ⁹⁵⁴ I8 Zhang, Y. S. *et al.* 3D extrusion bioprinting. *Nature Reviews Methods Primers* **1**, 75, doi:10.1038/s43586-021-00073-8 (2021).
- Guillemot, F., Mironov, V. & Nakamura, M. Bioprinting is coming of age: report from the International Conference on Bioprinting and Biofabrication in Bordeaux (3B'09).

 Biofabrication 2, 010201 (2010).
- Groll, J. *et al.* A definition of bioinks and their distinction from biomaterial inks. *Biofabrication* **11**, 013001 (2018).
- Zhou, X., Hou, Y. & Lin, J. A review on the processing accuracy of two-photon polymerization. *AIP Advances* **5**, 030701, doi:10.1063/1.4916886 (2015).
- Lee, M., Rizzo, R., Surman, F. & Zenobi-Wong, M. Guiding Lights: Tissue Bioprinting Using Photoactivated Materials. *Chem. Rev.* **120**, 10950-11027, doi:10.1021/acs.chemrev.0c00077 (2020).
- Harinarayana, V. & Shin, Y. C. Two-photon lithography for three-dimensional fabrication in micro/nanoscale regime: A comprehensive review. *Optics & Laser Technology* **142**, 107180 (2021).
- Skoog, S. A., Goering, P. L. & Narayan, R. J. Stereolithography in tissue engineering. *J. Mater. Sci. Mater. Med.* **25**, 845-856 (2014).
- Kuo, A. P. *et al.* High-Precision Stereolithography of Biomicrofluidic Devices. *Advanced Materials Technologies* **4**, 1800395, doi:https://doi.org/10.1002/admt.201800395 (2019).
- Li, H. *et al.* Digital light processing (DLP)-based (bio)printing strategies for tissue modeling and regeneration. *Aggregate* **n/a**, e270, doi:<u>https://doi.org/10.1002/agt2.270</u> (2022).
- Kowsari, K., Lee, W., Yoo, S.-S. & Fang, N. X. Scalable visible light 3D printing and bioprinting using an organic light-emitting diode microdisplay. *Iscience* **24**, 103372 (2021).
- Hosseinabadi, H. G. *et al.* Ink material selection and optical design considerations in DLP 3D printing. *Applied Materials Today* **30**, 101721 (2023).
- Lu, Y., Mapili, G., Suhali, G., Chen, S. & Roy, K. A digital micro-mirror device-based system for the microfabrication of complex, spatially patterned tissue engineering scaffolds. J. Biomed. Mater. Res. A. 77, 396-405 (2006).
- 983 30 Ma, X. *et al.* Deterministically patterned biomimetic human iPSC-derived hepatic model 984 via rapid 3D bioprinting. *Proct. Natl. Acad. Sci. U.S.A.* **113**, 2206-2211, 985 doi:10.1073/pnas.1524510113 (2016).
- Gauvin, R. *et al.* Microfabrication of complex porous tissue engineering scaffolds using 3D projection stereolithography. *Biomaterials* **33**, 3824-3834 (2012).
- Kelly, B. E. *et al.* Volumetric additive manufacturing via tomographic reconstruction. *Science* **363**, 1075-1079 (2019).

- Bernal, P. N. *et al.* Volumetric Bioprinting of Complex Living-Tissue Constructs within Seconds. *Adv. Mater.* **31**, 1904209, doi:https://doi.org/10.1002/adma.201904209 (2019).
- Bernal, P. N. *et al.* Volumetric Bioprinting of Organoids and Optically Tuned Hydrogels to Build Liver-Like Metabolic Biofactories. *Adv. Mater.* **34**, 2110054, doi:https://doi.org/10.1002/adma.202110054 (2022).
- Toombs, J. T. *et al.* Volumetric additive manufacturing of silica glass with microscale computed axial lithography. *Science* **376**, 308-312 (2022).
- Li, W. *et al.* Recent Advances in Formulating and Processing Biomaterial Inks for Vat Polymerization-Based 3D Printing. *Adv. Healthcare Mater.* **9**, 2000156, doi:10.1002/adhm.202000156 (2020).
- Murphy, C. A., Lim, K. S. & Woodfield, T. B. F. Next Evolution in Organ-Scale Biofabrication: Bioresin Design for Rapid High-Resolution Vat Polymerization. *Adv. Mater.* **34**, 2107759, doi:https://doi.org/10.1002/adma.202107759 (2022).
- Bader, C. *et al.* Making data matter: Voxel printing for the digital fabrication of data across scales and domains. *Science Advances* **4**, eaas8652, doi:10.1126/sciadv.aas8652.
- Hiller, J. & Lipson, H. Design and analysis of digital materials for physical 3D voxel printing. *Rapid Prototyping Journal* (2009).
- Wu, C., Yi, R., Liu, Y. J., He, Y. & Wang, C. C. L. in 2016 IEEE/RSJ International Conference on Intelligent Robots and Systems (IROS). 2155-2160.
- Huang, J., Ware, H. O. T., Hai, R., Shao, G. & Sun, C. Conformal Geometry and Multimaterial Additive Manufacturing through Freeform Transformation of Building Layers. *Adv. Mater.* **33**, 2005672, doi:https://doi.org/10.1002/adma.202005672 (2021).
- Kwok, T.-H. Comparing slicing technologies for digital light processing printing. *Journal* of Computing and Information Science in Engineering **19** (2019).
- Madrid-Wolff, J., Boniface, A., Loterie, D., Delrot, P. & Moser, C. Controlling Light in Scattering Materials for Volumetric Additive Manufacturing. *Advanced Science*, 2105144 (2022).
- 1017 44 *OpenExposer*, < https://hackaday.io/project/1129-openexposer> (
- de Beer, M. P. *et al.* Rapid, continuous additive manufacturing by volumetric polymerization inhibition patterning. *Science Advances* **5**, eaau8723, doi:10.1126/sciadv.aau8723 (2019).
- Lipkowitz, G. *et al.* Injection continuous liquid interface production of 3D objects. *Science Advances* **8**, eabq3917, doi:10.1126/sciadv.abq3917 (2022).
- Tumbleston, J. R. *et al.* Continuous liquid interface production of 3D objects. *Science* **347**, 1349 (2015).
- Wang, B. *et al.* Stiffness control in dual color tomographic volumetric 3D printing. *Nature Communications* **13**, 367, doi:10.1038/s41467-022-28013-4 (2022).
- Sameni, F. *et al.* Hot Lithography Vat Photopolymerisation 3D Printing: Vat Temperature vs. Mixture Design. *Polymers* **14**, 2988 (2022).
- Murphy, C. A., Lim, K. S. & Woodfield, T. B. F. Next Evolution in Organ-Scale Biofabrication: Bioresin Design for Rapid High-Resolution Vat Polymerization. *Adv Mater* **34**, e2107759, doi:10.1002/adma.202107759 (2022).
- Morgan, F. L. C., Moroni, L. & Baker, M. B. Dynamic Bioinks to Advance Bioprinting. Adv Healthc Mater 9, e1901798, doi:10.1002/adhm.201901798 (2020).

- Dong, Y. *et al.* Engineering the Cell Microenvironment Using Novel Photoresponsive Hydrogels. *ACS Appl Mater Interfaces* **10**, 12374-12389, doi:10.1021/acsami.7b17751 (2018).
- Adhikari, J. *et al.* Effects of Processing Parameters of 3D Bioprinting on the Cellular Activity of Bioinks. *Macromol Biosci* **21**, e2000179, doi:10.1002/mabi.202000179 (2021).
- Ng, W. L. *et al.* Vat polymerization-based bioprinting-process, materials, applications and regulatory challenges. *Biofabrication* **12**, 022001, doi:10.1088/1758-5090/ab6034 (2020).
- Shadish, J. A., Benuska, G. M. & DeForest, C. A. Bioactive site-specifically modified proteins for 4D patterning of gel biomaterials. *Nat. Mater* **18**, 1005-1014 (2019).
- Wang, B. *et al.* Stiffness control in dual color tomographic volumetric 3D printing. *Nat Commun* **13**, 367, doi:10.1038/s41467-022-28013-4 (2022).
- Wang, M. *et al.* Digital Light Processing-based Bioprinting with Composable Gradients. *Adv. Mater.* **34**, 2107038, doi: https://doi.org/10.1002/adma.202107038 (2022).
- Yu, C. *et al.* A sequential 3D bioprinting and orthogonal bioconjugation approach for precision tissue engineering. *Biomaterials* **258**, 120294 (2020).
- Ravanbakhsh, H., Bao, G., Luo, Z., Mongeau, L. G. & Zhang, Y. S. Composite Inks for Extrusion Printing of Biological and Biomedical Constructs. *ACS Biomaterials Science & Engineering* **7**, 4009-4026, doi:10.1021/acsbiomaterials.0c01158 (2021).
- Zhang, S. *et al.* Convergence of 3D Bioprinting and Nanotechnology in Tissue Engineering Scaffolds. *Biomimetics* **8**, 94 (2023).
- Loukelis, K., Helal, Z. A., Mikos, A. G. & Chatzinikolaidou, M. Nanocomposite Bioprinting for Tissue Engineering Applications. *Gels* **9**, 103 (2023).
- Alcala-Orozco, C. R. *et al.* Design and characterisation of multi-functional strontiumgelatin nanocomposite bioinks with improved print fidelity and osteogenic capacity. *Bioprinting* **18**, e00073 (2020).
- Li, L. *et al.* Methacrylate-Modified Gold Nanoparticles Enable Noninvasive Monitoring of Photocrosslinked Hydrogel Scaffolds. *Advanced NanoBiomed Research* **2**, 2200022 (2022).
- Tao, J. *et al.* Nanoparticle-stabilized emulsion bioink for digital light processing based 3D bioprinting of porous tissue constructs. *Adv. Healthcare Mater.* **11**, 2102810 (2022).
- Ouyang, L., Wojciechowski, J. P., Tang, J., Guo, Y. & Stevens, M. M. Tunable microgeltemplated porogel (MTP) bioink for 3D bioprinting applications. *Adv. Healthcare Mater.* 11, 2200027 (2022).
- Ying, G.-L. *et al.* Aqueous Two-Phase Emulsion Bioink-Enabled 3D Bioprinting of Porous Hydrogels. *Adv. Mater.* **30**, 1805460, doi:10.1002/adma.201805460 (2018).
- Yi, S. *et al.* Micropore-Forming Gelatin Methacryloyl (GelMA) Bioink Toolbox 2.0:
 Designable Tunability and Adaptability for 3D Bioprinting Applications. *Small* **18**, 2106357 (2022).
- Lim, K. S. *et al.* Fundamentals and Applications of Photo-Cross-Linking in Bioprinting. *Chem Rev* **120**, 10662-10694, doi:10.1021/acs.chemrev.9b00812 (2020).
- Tomal, W. & Ortyl, J. Water-Soluble Photoinitiators in Biomedical Applications. *Polymers* (*Basel*) **12**, doi:10.3390/polym12051073 (2020).
- Lim, K. S. *et al.* Visible Light Cross-Linking of Gelatin Hydrogels Offers an Enhanced Cell Microenvironment with Improved Light Penetration Depth. *Macromol. Biosci.* **19**, 1900098, doi:https://doi.org/10.1002/mabi.201900098 (2019).

- Wu, Y., Simpson, M. C. & Jin, J. Fast Hydrolytically Degradable 3D Printed Object Based on Aliphatic Polycarbonate Thiol Yne Photoresins. *Macromolecular Chemistry and Physics* **222**, doi:10.1002/macp.202000435 (2021).
- Tibbitt, M. W., Kloxin, A. M., Sawicki, L. & Anseth, K. S. Mechanical Properties and Degradation of Chain and Step Polymerized Photodegradable Hydrogels. *Macromolecules* **46**, 2785-2792, doi:10.1021/ma302522x (2013).
- 1085 73 Scinto, S. L. *et al.* Bioorthogonal chemistry. *Nat Rev Methods Primers* **1**, doi:10.1038/s43586-021-00028-z (2021).
- 74 Fairbanks, B. D. *et al.* Photoclick Chemistry: A Bright Idea. *Chem Rev* **121**, 6915-6990, doi:10.1021/acs.chemrev.0c01212 (2021).
- Albada, B., Keijzer, J. F., Zuilhof, H. & van Delft, F. Oxidation-Induced "One-Pot" Click Chemistry. *Chem Rev* **121**, 7032-7058, doi:10.1021/acs.chemrev.0c01180 (2021).
- Kim, H. *et al.* Light-Activated Decellularized Extracellular Matrix-Based Bioinks for Volumetric Tissue Analogs at the Centimeter Scale. *Adv. Funct. Mater.*, 2011252 (2021).
- Bjork, J. W., Johnson, S. L. & Tranquillo, R. T. Ruthenium-catalyzed photo cross-linking of fibrin-based engineered tissue. *Biomaterials* **32**, 2479-2488, doi:https://doi.org/10.1016/j.biomaterials.2010.12.010 (2011).
- Lim, K. S. *et al.* New Visible-Light Photoinitiating System for Improved Print Fidelity in Gelatin-Based Bioinks. *ACS Biomaterials Science & Engineering* **2**, 1752-1762, doi:10.1021/acsbiomaterials.6b00149 (2016).
- Soliman, B. G. *et al.* Programming Delayed Dissolution into Sacrificial Bioinks for Dynamic Temporal Control of Architecture within 3D-Bioprinted Constructs. *Adv. Funct. Mater.* (2023).
- Xie, M. *et al.* Volumetric Additive Manufacturing of Pristine Silk-Based (Bio)inks. *Nature Communications* **14**, 210 (2023).
- Rydholm, A. E., Bowman, C. N. & Anseth, K. S. Degradable thiol-acrylate photopolymers: polymerization and degradation behavior of an in situ forming biomaterial. *Biomaterials* **26**, 4495-4506, doi:10.1016/j.biomaterials.2004.11.046 (2005).
- Haris, U., Plank, J. T., Li, B., Page, Z. A. & Lippert, A. R. Visible Light Chemical Micropatterning Using a Digital Light Processing Fluorescence Microscope. *ACS Cent Sci* **8**, 67-76, doi:10.1021/acscentsci.1c01234 (2022).
- Rizzo, R., Ruetsche, D., Liu, H. & Zenobi-Wong, M. Optimized Photoclick (Bio)Resins for Fast Volumetric Bioprinting. *Adv. Mater.* 33, 2102900, doi:https://doi.org/10.1002/adma.202102900 (2021).
- Bertassoni, L. E. Bioprinting of Complex Multicellular Organs with Advanced Functionality-Recent Progress and Challenges Ahead. *Adv Mater* **34**, e2101321, doi:10.1002/adma.202101321 (2022).
- Dhand, A. P. *et al.* Simultaneous One-Pot Interpenetrating Network Formation to Expand 3D Processing Capabilities. *Adv Mater* **34**, e2202261, doi:10.1002/adma.202202261 (2022).
- Caprioli, M. *et al.* 3D-printed self-healing hydrogels via Digital Light Processing. *Nat Commun* **12**, 2462, doi:10.1038/s41467-021-22802-z (2021).
- Schwab, A. *et al.* Printability and Shape Fidelity of Bioinks in 3D Bioprinting. *Chem. Rev.* 1122
 120, 11028-11055, doi:10.1021/acs.chemrev.0c00084 (2020).

- Durand-Silva, A. *et al.* Balancing Self-Healing and Shape Stability in Dynamic Covalent Photoresins for Stereolithography 3D Printing. *ACS Macro Lett* **10**, 486-491, doi:10.1021/acsmacrolett.1c00121 (2021).
- Robinson, L. L. *et al.* Chemical and Mechanical Tunability of 3D-Printed Dynamic Covalent Networks Based on Boronate Esters. *ACS Macro Lett* **10**, 857-863, doi:10.1021/acsmacrolett.1c00257 (2021).
- Wilts, E. M. *et al.* Vat photopolymerization of charged monomers: 3D printing with supramolecular interactions. *Polymer Chemistry* **10**, 1442-1451, doi:10.1039/c8py01792a (2019).
- Uzcategui, A. C., Muralidharan, A., Ferguson, V. L., Bryant, S. J. & McLeod, R. R. Understanding and Improving Mechanical Properties in 3D printed Parts Using a Dual-Cure Acrylate-Based Resin for Stereolithography. *Adv Eng Mater* **20**, doi:10.1002/adem.201800876 (2018).
- Stevens, L. M., Tagnon, C. & Page, Z. A. "Invisible" Digital Light Processing 3D Printing with Near Infrared Light. *ACS Appl Mater Interfaces*, doi:10.1021/acsami.1c22046 (2022).
- Sanders, S. N. *et al.* Triplet fusion upconversion nanocapsules for volumetric 3D printing. *Nature* **604**, 474-478, doi:10.1038/s41586-022-04485-8 (2022).
- Thijssen, Q. *et al.* Volumetric Printing of Thiol-Ene Photo-Cross-Linkable Poly (ε-caprolactone): a Tunable Material Platform serving Biomedical Applications. *Adv. Mater.*, 2210136 (2023).
- Hahn, V. *et al.* Two-step absorption instead of two-photon absorption in 3D nanoprinting. *Nature Photonics* **15**, 932-938, doi:10.1038/s41566-021-00906-8 (2021).
- Hahn, V. *et al.* Light-sheet 3D microprinting via two-colour two-step absorption. *Nature Photonics* **16**, 784-791, doi:10.1038/s41566-022-01081-0 (2022).
- Mensov, S. N. *et al.* Use of photodegradable inhibitors in UV-curable compositions to form polymeric 2D-structures by visible light. *Journal of Applied Polymer Science* **137**, doi:10.1002/app.48976 (2020).
- Goodarzi Hosseinabadi, H., Dogan, E., Miri, A. K. & Ionov, L. Digital Light Processing Bioprinting Advances for Microtissue Models. *ACS Biomater Sci Eng* **8**, 1381-1395, doi:10.1021/acsbiomaterials.1c01509 (2022).
- You, S. *et al.* High Cell Density and High Resolution 3D Bioprinting for Fabricating Vascularized Tissues. *Science Advances* **9**, eade7923 (2023).
- Rizzo, R., Petelinšek, N., Bonato, A. & Zenobi-Wong, M. From Free-Radical to Radical-Free: A Paradigm Shift in Light-Mediated Biofabrication. *Advanced Science*, 2205302, doi:https://doi.org/10.1002/advs.202205302 (2023).
- 101 Bao, Y., Paunović, N. & Leroux, J. C. Challenges and Opportunities in 3D Printing of Biodegradable Medical Devices by Emerging Photopolymerization Techniques. *Advanced Functional Materials* **32**, doi:10.1002/adfm.202109864 (2022).
- 1161 102 Beh, C. W. *et al.* A fluid-supported 3D hydrogel bioprinting method. *Biomaterials* **276**, 121034, doi:10.1016/j.biomaterials.2021.121034 (2021).
- Brown, T. E. *et al.* Voxel-Scale Conversion Mapping Informs Intrinsic Resolution in Stereolithographic Additive Manufacturing. *ACS Applied Polymer Materials* **3**, 290-298, doi:10.1021/acsapm.0c01090 (2020).
- Salvekar, A. V. *et al.* Rapid Volumetric Additive Manufacturing in Solid State: A Demonstration to Produce Water-Content-Dependent Cooling/Heating/Water-Responsive

- Shape Memory Hydrogels. *3D Printing and Additive Manufacturing*, doi:10.1089/3dp.2021.0279 (2022).
- 105 Kloxin, A. M., Kasko, A. M., Salinas, C. N. & Anseth, K. S. Photodegradable hydrogels for dynamic tuning of physical and chemical properties. *Science* **324**, 59-63, doi:10.1126/science.1169494 (2009).
- McKinnon, D. D., Brown, T. E., Kyburz, K. A., Kiyotake, E. & Anseth, K. S. Design and characterization of a synthetically accessible, photodegradable hydrogel for user-directed formation of neural networks. *Biomacromolecules* **15**, 2808-2816 (2014).
- 107 Xie, R., Zheng, W., Guan, L., Ai, Y. & Liang, Q. Engineering of Hydrogel Materials with
 1177 Perfusable Microchannels for Building Vascularized Tissues. *Small* **16**, e1902838,
 1178 doi:10.1002/smll.201902838 (2020).
- Brown, T. E., Marozas, I. A. & Anseth, K. S. Amplified Photodegradation of Cell-Laden Hydrogels via an Addition-Fragmentation Chain Transfer Reaction. *Adv Mater* **29**, doi:10.1002/adma.201605001 (2017).
- Nelson, B. R. *et al.* Photoinduced Dithiolane Crosslinking for Multiresponsive Dynamic Hydrogels. *Adv. Mater.*, 2211209 (2023).
- Tavafoghi, M. *et al.* Multimaterial bioprinting and combination of processing techniques towards the fabrication of biomimetic tissues and organs. *Biofabrication* **13**, doi:10.1088/1758-5090/ac0b9a (2021).
- Davidson, M. D. *et al.* Programmable and contractile materials through cell encapsulation in fibrous hydrogel assemblies. *Sci Adv* 7, eabi8157, doi:10.1126/sciadv.abi8157 (2021).
- 1189 112 Carberry, B. J. *et al.* 3D printing of sacrificial thioester elastomers using digital light 1190 processing for templating 3D organoid structures in soft biomatrices. *Biofabrication* **13**, 1191 044104, doi:10.1088/1758-5090/ac1c98 (2021).
- Wang, M. *et al.* Molecularly cleavable bioinks facilitate high-performance digital light processing-based bioprinting of functional volumetric soft tissues. *Nature Communications* **13**, 3317 (2022).
- Levato, R. *et al.* High-resolution lithographic biofabrication of hydrogels with complex microchannels from low-temperature-soluble gelatin bioresins. *Materials Today Bio* **12**, 100162, doi:https://doi.org/10.1016/j.mtbio.2021.100162 (2021).
- 115 Müller, M. Z., Style, R. W., Müller, R. & Qin, X.-H. A Phase-separating Thiol-ene Photoresin for Volumetric Bioprinting of Macroporous Hydrogels. *bioRxiv*, 2022.2001.2029.478338, doi:10.1101/2022.01.29.478338 (2022).
- 116 Qin, X.-S., Wang, M., Li, W. & Zhang, Y. S. Biosurfactant-Stabilized Micropore-Forming
 1202 GelMA Inks Enable Improved Usability for 3D Printing Applications. Regenerative
 1203 Engineering and Translational Medicine 8, 471-481 (2022).
- Sampson, K. L. *et al.* Multimaterial Vat Polymerization Additive Manufacturing. *ACS Applied Polymer Materials* **3**, 4304-4324, doi:10.1021/acsapm.1c00262 (2021).
- 1206 118 Ravanbakhsh, H. *et al.* Emerging Technologies in Multi-Material Bioprinting. *Adv. Mater.* 1207 33, 2104730, doi:10.1002/adma.202104730 (2021).
- 1208 119 Choi, J.-W., Kim, H.-C. & Wicker, R. Multi-material stereolithography. *J. Mater. Process.*1209 *Technol.* **211**, 318-328 (2011).
- Grigoryan, B. *et al.* Development, characterization, and applications of multi-material stereolithography bioprinting. *Sci. Rep.* **11**, 3171, doi:10.1038/s41598-021-82102-w (2021).
- 121 Liao, J. et al. 3D-Printable Colloidal Photonic Crystals. Mater. Today 56, 29-41 (2022).

- 1214 122 Cheng, J. *et al.* Centrifugal multimaterial 3D printing of multifunctional heterogeneous objects. *Nature Communications* **13**, 7931, doi:10.1038/s41467-022-35622-6 (2022).
- Miri, A. K. *et al.* Microfluidics-Enabled Multimaterial Maskless Stereolithographic Bioprinting. *Adv. Mater.* **30**, 1800242, doi:10.1002/adma.201800242 (2018).
- Han, D., Yang, C., Fang, N. X. & Lee, H. Rapid multi-material 3D printing with projection micro-stereolithography using dynamic fluidic control. *Additive Manufacturing* **27**, 606-615, doi:https://doi.org/10.1016/j.addma.2019.03.031 (2019).
- Liu, J., Hwang, H. H., Wang, P., Whang, G. & Chen, S. Direct 3D-printing of cell-laden constructs in microfluidic architectures. *Lab Chip* **16**, 1430-1438 (2016).
- 1223 126 Chansoria, P. *et al.* Synergizing algorithmic design, photoclick chemistry and multi-1224 material volumetric printing for accelerating complex shape engineering. *bioRxiv*, 1225 2022.2011.2029.518318, doi:10.1101/2022.11.29.518318 (2022).
- 127 Bialas, S. *et al.* Access to Disparate Soft Matter Materials by Curing with Two Colors of Light. *Adv. Mater.* **31**, 1807288, doi: https://doi.org/10.1002/adma.201807288 (2019).
- 128 Schwartz, J. J. & Boydston, A. J. Multimaterial actinic spatial control 3D and 4D printing.

 Nature communications 10, 791-791, doi:10.1038/s41467-019-08639-7 (2019).
- Peng, X. *et al.* Multi-Color 3D Printing via Single-Vat Grayscale Digital Light Processing. *Adv. Funct. Mater.* **32**, 2112329, doi:https://doi.org/10.1002/adfm.202112329 (2022).
- Kuang, X. et al. Grayscale digital light processing 3D printing for highly functionally graded materials. Science advances 5, eaav5790 (2019).
- Yue, L. *et al.* Single-vat single-cure grayscale digital light processing 3D printing of materials with large property difference and high stretchability. *Nature Communications* 14, 1251, doi:10.1038/s41467-023-36909-y (2023).
- Shanjani, Y., Pan, C. C., Elomaa, L. & Yang, Y. A novel bioprinting method and system for forming hybrid tissue engineering constructs. *Biofabrication* 7, 045008, doi:10.1088/1758-5090/7/4/045008 (2015).
- 133 An, H. S. *et al.* High-Resolution 3D Printing of Freeform, Transparent Displays in Ambient Air. *Advanced Science* **6**, 1901603, doi: https://doi.org/10.1002/advs.201901603 (2019).
- Greenhall, J. & Raeymaekers, B. 3D Printing Macroscale Engineered Materials Using Ultrasound Directed Self-Assembly and Stereolithography. *Advanced Materials Technologies* **2**, 1700122, doi:https://doi.org/10.1002/admt.201700122 (2017).
- Lu, L., Tang, X., Hu, S. & Pan, Y. Acoustic Field-Assisted Particle Patterning for Smart Polymer Composite Fabrication in Stereolithography. 3D Printing and Additive Manufacturing 5, 151-159, doi:10.1089/3dp.2017.0157 (2018).
- Wang, Y. *et al.* Acoustic-assisted 3D printing based on acoustofluidic microparticles patterning for conductive polymer composites fabrication. *Additive Manufacturing* **60**, 103247, doi:https://doi.org/10.1016/j.addma.2022.103247 (2022).
- 1251 Kunwar, P. et al. Hybrid Laser Printing of 3D, Multiscale, Multimaterial Hydrogel
 1252 Structures. Advanced Optical Materials 7, 1900656,
 1253 doi:https://doi.org/10.1002/adom.201900656 (2019).
- 138 Rizzo, R. *et al.* Multiscale Hybrid Fabrication: Volumetric Printing Meets Two-Photon Ablation. *bioRxiv*, 2022.2010.2028.513651, doi:10.1101/2022.10.28.513651 (2022).
- Größbacher, G. *et al.* Volumetric Printing across Melt Electrowritten Scaffolds Fabricates Multi-Material Living Constructs with Tunable Architecture and Mechanics. *bioRxiv*, 2023.2001.2024.525418, doi:10.1101/2023.01.24.525418 (2023).

- Huh, J. *et al.* Combinations of photoinitiator and UV absorber for cell-based digital light processing (DLP) bioprinting. *Biofabrication* **13**, 034103, doi:10.1088/1758-5090/abfd7a (2021).
- Bennett, J. Measuring UV curing parameters of commercial photopolymers used in additive manufacturing. *Additive manufacturing* **18**, 203-212 (2017).
- Seck, T. M., Melchels, F. P. W., Feijen, J. & Grijpma, D. W. Designed biodegradable hydrogel structures prepared by stereolithography using poly (ethylene glycol)/poly (d, l-lactide)-based resins. *Journal of Controlled Release* **148**, 34-41 (2010).
- Van Hoorick, J. *et al.* Cross-linkable gelatins with superior mechanical properties through carboxylic acid modification: increasing the two-photon polymerization potential. *Biomacromolecules* **18**, 3260-3272 (2017).
- Galarraga, J. H., Dhand, A. P., Enzmann, B. P., III & Burdick, J. A. Synthesis, Characterization, and Digital Light Processing of a Hydrolytically Degradable Hyaluronic Acid Hydrogel. *Biomacromolecules* **24**, 413-425, doi:10.1021/acs.biomac.2c01218 (2023).
- Sanchez Noriega, J. L. *et al.* Spatially and optically tailored 3D printing for highly miniaturized and integrated microfluidics. *Nature Communications* **12**, 5509, doi:10.1038/s41467-021-25788-w (2021).
- Grigoryan, B. *et al.* Multivascular networks and functional intravascular topologies within biocompatible hydrogels. *Science* **364**, 458, doi:10.1126/science.aav9750 (2019).
- 147 Khoon, S. L. *et al.* Bio-resin for high resolution lithography-based biofabrication of complex cell-laden constructs. *Biofabrication* **10**, 034101 (2018).
- Janusziewicz, R., Tumbleston, J. R., Quintanilla, A. L., Mecham, S. J. & DeSimone, J. M. Layerless fabrication with continuous liquid interface production. *Proct. Natl. Acad. Sci. U.S.A.* **113**, 11703-11708, doi:10.1073/pnas.1605271113 (2016).
- Loterie, D., Delrot, P. & Moser, C. High-resolution tomographic volumetric additive manufacturing. *Nature communications* **11**, 1-6 (2020).
- Salajeghe, R., Meile, D. H., Kruse, C. S., Marla, D. & Spangenberg, J. Numerical Modeling of Part Sedimentation During Volumetric Additive Manufacturing. *Available at SSRN* 4229359 (2022).
- Caliari, S. R. & Burdick, J. A. A practical guide to hydrogels for cell culture. *Nat. Methods* 13, 405-414, doi:10.1038/nmeth.3839 (2016).
- Fedorovich, N. E. *et al.* The effect of photopolymerization on stem cells embedded in hydrogels. *Biomaterials* **30**, 344-353, doi:https://doi.org/10.1016/j.biomaterials.2008.09.037 (2009).
- Ruskowitz, E. R. & DeForest, C. A. Proteome-wide Analysis of Cellular Response to Ultraviolet Light for Biomaterial Synthesis and Modification. *ACS Biomaterials Science & Engineering* **5**, 2111-2116, doi:10.1021/acsbiomaterials.9b00177 (2019).
- Bartnikowski, M., Bartnikowski, N. J., Woodruff, M. A., Schrobback, K. & Klein, T. J. Protective effects of reactive functional groups on chondrocytes in photocrosslinkable hydrogel systems. *Acta Biomater.* **27**, 66-76 (2015).
- 1299 155 Kratochvil, M. J. *et al.* Engineered materials for organoid systems. *Nature Reviews*1300 *Materials* **4**, 606-622, doi:10.1038/s41578-019-0129-9 (2019).
- Ovsianikov, A., Mironov, V., Stampfl, J. & Liska, R. Engineering 3D cell-culture matrices: multiphoton processing technologies for biological and tissue engineering applications. Expert Review of Medical Devices 9, 613-633, doi:10.1586/erd.12.48 (2012).

- Dobos, A. *et al.* On-chip high-definition bioprinting of microvascular structures. *Biofabrication* **13**, 015016, doi:10.1088/1758-5090/abb063 (2021).
- Marino, A. *et al.* The Osteoprint: a bioinspired two-photon polymerized 3-D structure for the enhancement of bone-like cell differentiation. *Acta Biomater.* **10**, 4304-4313 (2014).
- Marino, A. *et al.* A 3D real-scale, biomimetic, and biohybrid model of the blood-brain barrier fabricated through two-photon lithography. *Small* **14**, 1702959 (2018).
- Krüger, H., Asido, M., Wachtveitl, J., Tampé, R. & Wieneke, R. Sensitizer-enhanced two-photon patterning of biomolecules in photoinstructive hydrogels. *Communications Materials* 3, 9, doi:10.1038/s43246-022-00230-w (2022).
- Broguiere, N. et al. Morphogenesis Guided by 3D Patterning of Growth Factors in Biological Matrices. Advanced Materials 32, 1908299, doi:https://doi.org/10.1002/adma.201908299 (2020).
- Qin, X.-H., Wang, X., Rottmar, M., Nelson, B. J. & Maniura-Weber, K. Near-Infrared Light-Sensitive Polyvinyl Alcohol Hydrogel Photoresist for Spatiotemporal Control of Cell-Instructive 3D Microenvironments. *Advanced Materials* **30**, 1705564, doi:https://doi.org/10.1002/adma.201705564 (2018).
- 1320 163 Skylar-Scott, M. A., Liu, M. C., Wu, Y., Dixit, A. & Yanik, M. F. Guided Homing of Cells 1321 in Multi-Photon Microfabricated Bioscaffolds. *Adv. Healthcare Mater.* **5**, 1233-1243 1322 (2016).
- DeForest, C. A. & Anseth, K. S. Cytocompatible click-based hydrogels with dynamically tunable properties through orthogonal photoconjugation and photocleavage reactions.

 Nature Chemistry 3, 925-931, doi:10.1038/nchem.1174 (2011).
- Arakawa, C. K., Badeau, B. A., Zheng, Y. & DeForest, C. A. Multicellular Vascularized Engineered Tissues through User-Programmable Biomaterial Photodegradation. *Advanced Materials* **29**, 1703156, doi:https://doi.org/10.1002/adma.201703156 (2017).
- 1329 166 Rayner, S. G. *et al.* Multiphoton-Guided Creation of Complex Organ-Specific Microvasculature. *Advanced Healthcare Materials* **10**, 2100031, doi:https://doi.org/10.1002/adhm.202100031 (2021).
- 1332 167 Enrico, A. *et al.* 3D Microvascularized Tissue Models by Laser-Based Cavitation Molding 1333 of Collagen. *Advanced Materials* **34**, 2109823, 1334 doi:https://doi.org/10.1002/adma.202109823 (2022).
- Marino, A. *et al.* A 3D Real-Scale, Biomimetic, and Biohybrid Model of the Blood-Brain Barrier Fabricated through Two-Photon Lithography. *Small* **14**, 1702959, doi:https://doi.org/10.1002/smll.201702959 (2018).
- Skylar-Scott, M. A., Liu, M.-C., Wu, Y., Dixit, A. & Yanik, M. F. Guided Homing of Cells in Multi-Photon Microfabricated Bioscaffolds. *Advanced Healthcare Materials* **5**, 1233-1243, doi:https://doi.org/10.1002/adhm.201600082 (2016).
- Ovsianikov, A. *et al.* Laser Photofabrication of Cell-Containing Hydrogel Constructs. Langmuir **30**, 3787-3794, doi:10.1021/la402346z (2014).
- Tromayer, M. *et al.* A biocompatible macromolecular two-photon initiator based on hyaluronan. *Polymer Chemistry* **8**, 451-460, doi:10.1039/C6PY01787H (2017).
- Tromayer, M. *et al.* A biocompatible diazosulfonate initiator for direct encapsulation of human stem cells via two-photon polymerization. *Polymer Chemistry* **9**, 3108-3117, doi:10.1039/C8PY00278A (2018).

- Lee, S. *et al.* A Needle-Type Microrobot for Targeted Drug Delivery by Affixing to a Microtissue. *Advanced Healthcare Materials* **9**, 1901697, doi:https://doi.org/10.1002/adhm.201901697 (2020).
- Cabanach, P. *et al.* Zwitterionic 3D-Printed Non-Immunogenic Stealth Microrobots. *Advanced Materials* **32**, 2003013, doi:https://doi.org/10.1002/adma.202003013 (2020).
- 1353 Ceylan, H. *et al.* 3D-Printed Biodegradable Microswimmer for Theranostic Cargo Delivery and Release. *ACS Nano* **13**, 3353-3362, doi:10.1021/acsnano.8b09233 (2019).
- Yasa, I. C., Tabak, A. F., Yasa, O., Ceylan, H. & Sitti, M. 3D-Printed Microrobotic Transporters with Recapitulated Stem Cell Niche for Programmable and Active Cell Delivery. *Advanced Functional Materials* **29**, 1808992, doi:https://doi.org/10.1002/adfm.201808992 (2019).
- Cordeiro, A. S. *et al.* Two-Photon Polymerisation 3D Printing of Microneedle Array Templates with Versatile Designs: Application in the Development of Polymeric Drug Delivery Systems. *Pharmaceutical Research* **37**, 174, doi:10.1007/s11095-020-02887-9 (2020).
- Lemma, E. D., Spagnolo, B., De Vittorio, M. & Pisanello, F. Studying Cell Mechanobiology in 3D: The Two-Photon Lithography Approach. *Trends in Biotechnology* 37, 358-372, doi:https://doi.org/10.1016/j.tibtech.2018.09.008 (2019).
- Tibbitt, M. W., Kloxin, A. M., Dyamenahalli, K. U. & Anseth, K. S. Controlled two-photon photodegradation of PEG hydrogels to study and manipulate subcellular interactions on soft materials. *Soft Matter* **6**, 5100-5108, doi:10.1039/C0SM00174K (2010).
- 180 Urciuolo, A. *et al.* Intravital three-dimensional bioprinting. *Nature Biomedical Engineering*, 901-915 (2020).
- 181 Abele, T. *et al.* Two-Photon 3D Laser Printing Inside Synthetic Cells. *Advanced Materials* 34, 2106709, doi: https://doi.org/10.1002/adma.202106709 (2022).
- Zhong, Z. *et al.* Rapid 3D bioprinting of a multicellular model recapitulating pterygium microenvironment. *Biomaterials* **282**, 121391 (2022).
- Soliman, B. G. *et al.* Development and Characterization of Gelatin-Norbornene Bioink to Understand the Interplay between Physical Architecture and Micro-Capillary Formation in Biofabricated Vascularized Constructs. *Advanced Healthcare Materials* **11**, 2101873, doi:https://doi.org/10.1002/adhm.202101873 (2022).
- Sun, A. X., Lin, H., Beck, A. M., Kilroy, E. J. & Tuan, R. S. Projection Stereolithographic Fabrication of Human Adipose Stem Cell-Incorporated Biodegradable Scaffolds for Cartilage Tissue Engineering. *Frontiers in Bioengineering and Biotechnology* 3, doi:10.3389/fbioe.2015.00115 (2015).
- He, B. *et al.* 3D printed biomimetic epithelium/stroma bilayer hydrogel implant for corneal regeneration. *Bioactive Materials* 17, 234-247, doi:https://doi.org/10.1016/j.bioactmat.2022.01.034 (2022).
- Elomaa, L. *et al.* Three-dimensional fabrication of cell-laden biodegradable poly(ethylene glycol-co-depsipeptide) hydrogels by visible light stereolithography. *Journal of Materials Chemistry B* **3**, 8348-8358, doi:10.1039/C5TB01468A (2015).
- Zhu, W. *et al.* Direct 3D bioprinting of prevascularized tissue constructs with complex microarchitecture. *Biomaterials* **124**, 106-115, doi:https://doi.org/10.1016/j.biomaterials.2017.01.042 (2017).

- Kiratitanaporn, W. *et al.* 3D printing a biocompatible elastomer for modeling muscle regeneration after volumetric muscle loss. *Biomaterials Advances* **142**, 213171, doi:https://doi.org/10.1016/j.bioadv.2022.213171 (2022).
- Ma, X. *et al.* Rapid 3D bioprinting of decellularized extracellular matrix with regionally varied mechanical properties and biomimetic microarchitecture. *Biomaterials* **185**, 310-321, doi:https://doi.org/10.1016/j.biomaterials.2018.09.026 (2018).
- 1398 190 Grix, T. *et al.* Bioprinting Perfusion-Enabled Liver Equivalents for Advanced Organ-ona-Chip Applications. *Genes* **9** (2018).
- 1400 191 Ma, Y. et al. Biomacromolecule-based agent for high-precision light-based 3D hydrogel 1401 bioprinting. Cell Reports Physical Science 3, 100985, 1402 doi:https://doi.org/10.1016/j.xcrp.2022.100985 (2022).
- Kim, S. H. *et al.* Precisely printable and biocompatible silk fibroin bioink for digital light processing 3D printing. *Nature Communications* **9**, 1620, doi:10.1038/s41467-018-03759-y (2018).
- Tang, M. *et al.* Three-dimensional bioprinted glioblastoma microenvironments model cellular dependencies and immune interactions. *Cell Res.* **30**, 833-853 (2020).
- Hos 194 Bracaglia, L. G. *et al.* 3D Printed Pericardium Hydrogels To Promote Wound Healing in Vascular Applications. *Biomacromolecules* 18, 3802-3811, doi:10.1021/acs.biomac.7b01165 (2017).
- Grigoryan, B. *et al.* Multivascular networks and functional intravascular topologies within biocompatible hydrogels. *Science* **364**, 458-464, doi:10.1126/science.aav9750 (2019).
 - 196 Rock Hill, South Carolina (ed 3D Systems Corporation) (2021).

- 1414 197 Anandakrishnan, N. *et al.* Fast Stereolithography Printing of Large-Scale Biocompatible
 1415 Hydrogel Models. *Adv. Healthcare Mater.* **10**, 2002103,
 1416 doi:https://doi.org/10.1002/adhm.202002103 (2021).
- Shopperly, L. K. *et al.* Blends of gelatin and hyaluronic acid stratified by stereolithographic bioprinting approximate cartilaginous matrix gradients. *Journal of Biomedical Materials Research Part B: Applied Biomaterials* 110, 2310-2322, doi:https://doi.org/10.1002/jbm.b.35079 (2022).
- 1421 199 Xie, C. *et al.* High-efficient engineering of osteo-callus organoids for rapid bone regeneration within one month. *Biomaterials* **288**, 121741 (2022).
- Tang, M. *et al.* Three-dimensional bioprinted glioblastoma microenvironments model cellular dependencies and immune interactions. *Cell Res.* **30**, 833-853, doi:10.1038/s41422-020-0338-1 (2020).
- Grix, T. *et al.* Bioprinting perfusion-enabled liver equivalents for advanced organ-on-a-chip applications. *Genes* **9**, 176 (2018).
- Ma, Y. *et al.* Biomacromolecule-based agent for high-precision light-based 3D hydrogel bioprinting. *Cell Reports Physical Science* **3**, 100985 (2022).
- Yang, H. *et al.* Fabricating hydrogels to mimic biological tissues of complex shapes and high fatigue resistance. *Matter* **4**, 1935-1946, doi:https://doi.org/10.1016/j.matt.2021.03.011 (2021).
- Wei, Y. *et al.* Stereolithography-based additive manufacturing of high-performance osteoinductive calcium phosphate ceramics by a digital light-processing system. *ACS biomaterials science & engineering* **6**, 1787-1797 (2020).

- Zhang, B. *et al.* Three-dimensional printing of large-scale, high-resolution bioceramics with micronano inner porosity and customized surface characterization design for bone regeneration. *ACS Appl. Mater. Interfaces* **14**, 8804-8815 (2022).
- de Oliveira, M. F., da Silva, L. C. E. & de Oliveira, M. G. 3D printed bioresorbable nitric oxide-releasing vascular stents. *Bioprinting* 22, e00137, doi:https://doi.org/10.1016/j.bprint.2021.e00137 (2021).
- Zhu, W. *et al.* Rapid continuous 3D printing of customizable peripheral nerve guidance conduits. *Materials Today* **21**, 951-959, doi:https://doi.org/10.1016/j.mattod.2018.04.001 (2018).
- Tao, J. *et al.* Rapid 3D printing of functional nanoparticle-enhanced conduits for effective nerve repair. *Acta Biomaterialia* **90**, 49-59, doi:https://doi.org/10.1016/j.actbio.2019.03.047 (2019).
- Koffler, J. *et al.* Biomimetic 3D-printed scaffolds for spinal cord injury repair. *Nat. Med.* **25**, 263-269 (2019).
- Liu, H. *et al.* Filamented Light (FLight) Biofabrication of Highly Aligned Tissue-Engineered Constructs. *Advanced Materials* **n/a**, 2204301, doi:https://doi.org/10.1002/adma.202204301 (2022).
- 1453 211 Chen, Y. et al. Noninvasive in vivo 3D bioprinting. Science Advances 6, eaba7406 (2020).
- Wang, Y. *et al.* 4D Printed Cardiac Construct with Aligned Myofibers and Adjustable Curvature for Myocardial Regeneration. *ACS Applied Materials & Interfaces* **13**, 12746-12758, doi:10.1021/acsami.0c17610 (2021).
- Dong, M. *et al.* Digital Light Processing 3D Printing of Tough Supramolecular Hydrogels with Sophisticated Architectures as Impact-Absorption Elements. *Advanced Materials* **34**, 2204333, doi:https://doi.org/10.1002/adma.202204333 (2022).
- Xue, D., Zhang, J., Wang, Y. & Mei, D. Digital Light Processing-Based 3D Printing of Cell-Seeding Hydrogel Scaffolds with Regionally Varied Stiffness. *ACS Biomaterials Science & Engineering* **5**, 4825-4833, doi:10.1021/acsbiomaterials.9b00696 (2019).
- Gehlen, J., Qiu, W., Schädli, G. N., Müller, R. & Qin, X.-H. Tomographic volumetric bioprinting of heterocellular bone-like tissues in seconds. *Acta Biomaterialia*, doi:https://doi.org/10.1016/j.actbio.2022.06.020 (2022).
- Wolf, K. J., Weiss, J. D., Uzel, S. G. M., Skylar-Scott, M. A. & Lewis, J. A. Biomanufacturing human tissues via organ building blocks. *Cell Stem Cell* **29**, 667-677, doi:https://doi.org/10.1016/j.stem.2022.04.012 (2022).
- 1469 217 Rackson, C. M. *et al.* Latent image volumetric additive manufacturing. *Opt. Lett.* **47**, 1279-1282, doi:10.1364/OL.449220 (2022).
- van der Laan, H. L., Burns, M. A. & Scott, T. F. Volumetric Photopolymerization Confinement through Dual-Wavelength Photoinitiation and Photoinhibition. *ACS Macro Letters* **8**, 899-904, doi:10.1021/acsmacrolett.9b00412 (2019).
- Rackson, C. M. *et al.* Object-space optimization of tomographic reconstructions for additive manufacturing. *Additive Manufacturing* **48**, 102367, doi:https://doi.org/10.1016/j.addma.2021.102367 (2021).
- Corbett, D. C. *et al.* Thermofluidic heat exchangers for actuation of transcription in artificial tissues. *Science advances* **6**, eabb9062 (2020).
- Walker David, A., Hedrick James, L. & Mirkin Chad, A. Rapid, large-volume, thermally controlled 3D printing using a mobile liquid interface. *Science* **366**, 360-364, doi:10.1126/science.aax1562 (2019).

- Madrid-Sánchez, A. *et al.* Fabrication of large-scale scaffolds with microscale features using light sheet stereolithography. *International Journal of Bioprinting; Vol 9, No 2* (2023)DO 10.18063/ijb.v9i2.650 (2022).
- Geng, Q., Wang, D., Chen, P. & Chen, S.-C. Ultrafast multi-focus 3-D nano-fabrication based on two-photon polymerization. *Nature Communications* **10**, 2179, doi:10.1038/s41467-019-10249-2 (2019).
- Maibohm, C. *et al.* Multi-beam two-photon polymerization for fast large area 3D periodic structure fabrication for bioapplications. *Sci. Rep.* **10**, 8740, doi:10.1038/s41598-020-64955-9 (2020).
- Oran, D. *et al.* 3D nanofabrication by volumetric deposition and controlled shrinkage of patterned scaffolds. *Science* **362**, 1281-1285 (2018).
- Gong, J. *et al.* Complexation-Induced Resolution Enhancement of 3D-Printed Hydrogel Constructs. *Nature Communications* **11**, 1267 (2020).
- Wang, M., Li, W., Garciamendez-Mijares, C. E. & Zhang, Y. S. Engineering (Bio)Materials through Shrinkage and Expansion. *Adv. Healthcare Mater.* **21**, 2100380 (2021).
- Chung Li, C., Toombs, J. & Taylor, H. in SCF '20: Proceedings of the 5th Annual ACM Symposium on Computational Fabrication. 1-7.
- You, S., Wang, P., Schimelman, J., Hwang, H. H. & Chen, S. High-fidelity 3D printing using flashing photopolymerization. *Additive manufacturing* **30**, 100834 (2019).
- Guan, J. *et al.* Compensating the cell-induced light scattering effect in light-based bioprinting using deep learning. *Biofabrication* **14**, 015011 (2021).
- You, S. *et al.* Mitigating scattering effects in light-based three-dimensional printing using machine learning. *Journal of Manufacturing Science and Engineering* **142**, 081002 (2020).
- Hsiao, K. *et al.* Single-digit-micrometer-resolution continuous liquid interface production. *Science Advances* **8**, eabq2846 (2022).
- Administration, U. S. F. D. Discussion Paper: 3D Printing Medical Devices at the Point of Care. (2021).
- Tahayeri, A. *et al.* 3D printed versus conventionally cured provisional crown and bridge dental materials. *Dent. Mater.* **34**, 192-200 (2018).
- Liaw, C.-Y. & Guvendiren, M. Current and emerging applications of 3D printing in medicine. *Biofabrication* **9**, 024102 (2017).
- Shen, E. M. & McCloskey, K. E. Affordable, high-resolution bioprinting with embedded concentration gradients. *Bioprinting* 21, e00113, doi:https://doi.org/10.1016/j.bprint.2020.e00113 (2021).
- Malda, J. *et al.* 25th Anniversary Article: Engineering Hydrogels for Biofabrication. *Adv. Mater.* 25, 5011-5028, doi:10.1002/adma.201302042 (2013).
- Noor, N. *et al.* 3D Printing of Personalized Thick and Perfusable Cardiac Patches and Hearts. *Advanced Science* **6**, 1900344, doi:https://doi.org/10.1002/advs.201900344 (2019).
- Mouser, V. H. M. *et al.* Yield stress determines bioprintability of hydrogels based on gelatin-methacryloyl and gellan gum for cartilage bioprinting. *Biofabrication* **8**, 035003, doi:10.1088/1758-5090/8/3/035003 (2016).
- Murphy, C. A., Lim, K. S. & Woodfield, T. B. F. Next Evolution in Organ-Scale Biofabrication: Bioresin Design for Rapid High-Resolution Vat Polymerization. *Adv. Mater.* **34**, 2107759 (2022).

- Sharaf, A. *et al.* Two-photon polymerization of 2.5 D and 3D microstructures fostering a ramified resting phenotype in primary microglia. *Frontiers in Bioengineering and Biotechnology* **10**, 926642 (2022).
- Arcaute, K., Mann, B. K. & Wicker, R. B. Stereolithography of Three-Dimensional Bioactive Poly(Ethylene Glycol) Constructs with Encapsulated Cells. *Ann. Biomed. Eng.* 34, 1429-1441, doi:10.1007/s10439-006-9156-y (2006).
- Arcaute, K., Mann, B. K. & Wicker, R. B. Fabrication of off-the-shelf multilumen poly (ethylene glycol) nerve guidance conduits using stereolithography. *Tissue Eng. C* **17**, 27-38 (2011).
- Rakin, R. H. *et al.* Tunable metacrylated hyaluronic acid-based hybrid bioinks for stereolithography 3D bioprinting. *Biofabrication* **13**, 044109 (2021).

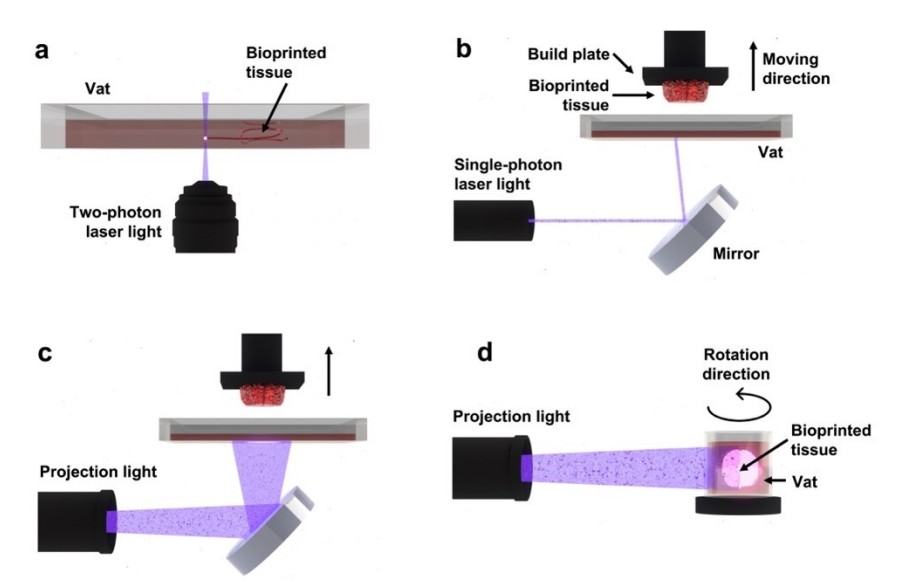


Fig. 1 | **Typical light-based vat-polymerization techniques. a** | TPL that raster-scans two-photon lasers to polymerize or deconstruct a bioresin for 3D bioprinting. **b** | SLA that raster-scans a single-photon laser for 3D bioprinting. **c** | DLP that projects a series of light patterns to achieve layer-by-layer 3D bioprinting. The system shown is the bottom-up configuration. **d** | Tomographic bioprinting that projects a series of intensity-modulated light patterns to achieve rotational 3D bioprinting.

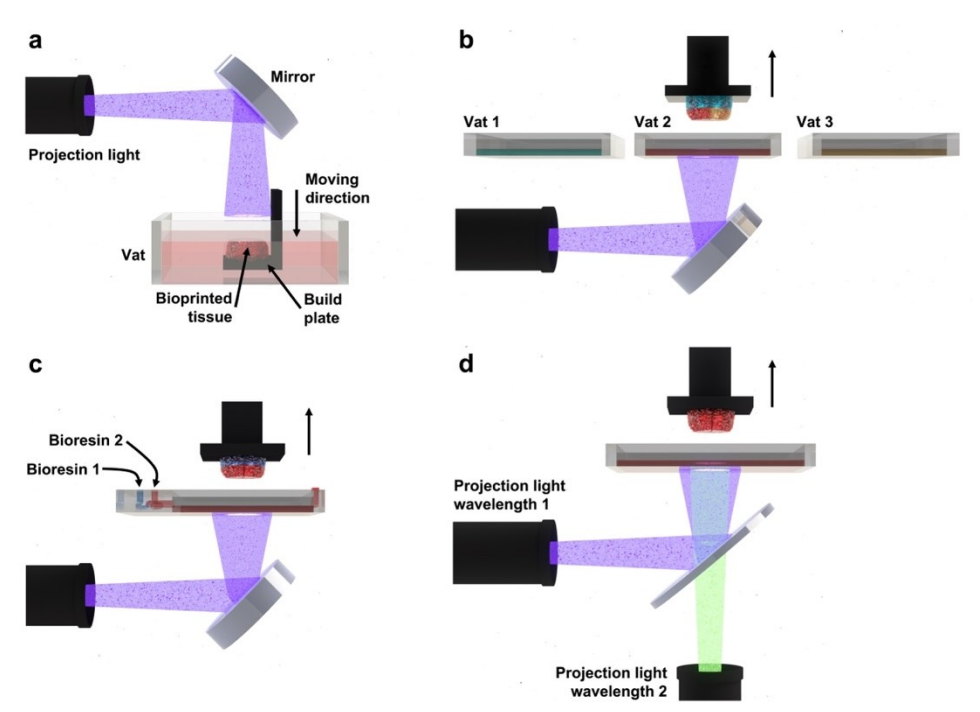


Fig. 2 | Variations in vat-polymerization techniques, taking DLP bioprinting as an example. $\mathbf{a} \mid \text{DLP}$ bioprinting in the top-down configuration. $\mathbf{b} \mid \text{Multi-material DLP}$ bioprinting using multiple vats. $\mathbf{c} \mid \text{Multi-material DLP}$ bioprinting using automated bioresin change through a microfluidics-integrated vat. $\mathbf{d} \mid \text{Heterogeneous-material DLP}$ bioprinting using multiple wavelengths.

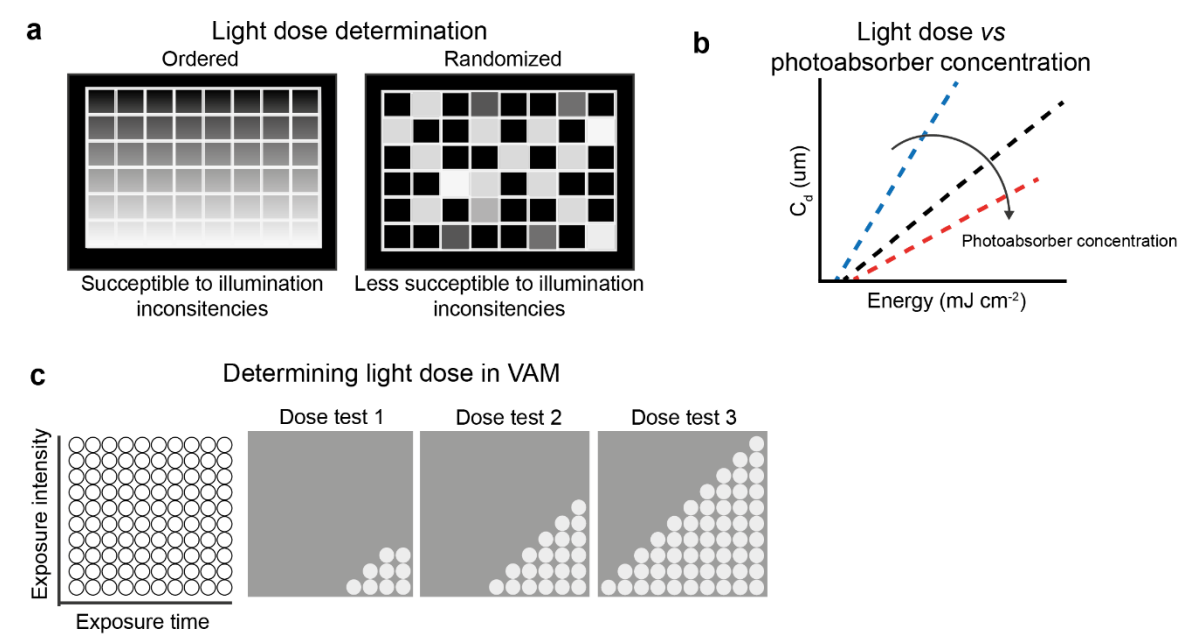


Fig. 3. Determining light-dose responses and working curves in light-based vatpolymerization bioprinting. $\bf a \mid A$ simple method to establish the SLA/DLP working curves consist of projecting an array of disks or squares onto the bioresin vat where each of those is exposed to an increasing light dose. $\bf b \mid A$ fter crosslinking, the thicknesses of the bioresin layer are measured and recorded to create a light energy *versus* thickness plot that can be used to construct the working curves. $\bf c \mid A$ dose test is performed to identify ideal light exposure parameters for tomographic bioprinting, by projecting an array of disk-shaped spots within cuvette containing the bioresin, with each spot corresponding to a varying light intensity and exposure time.

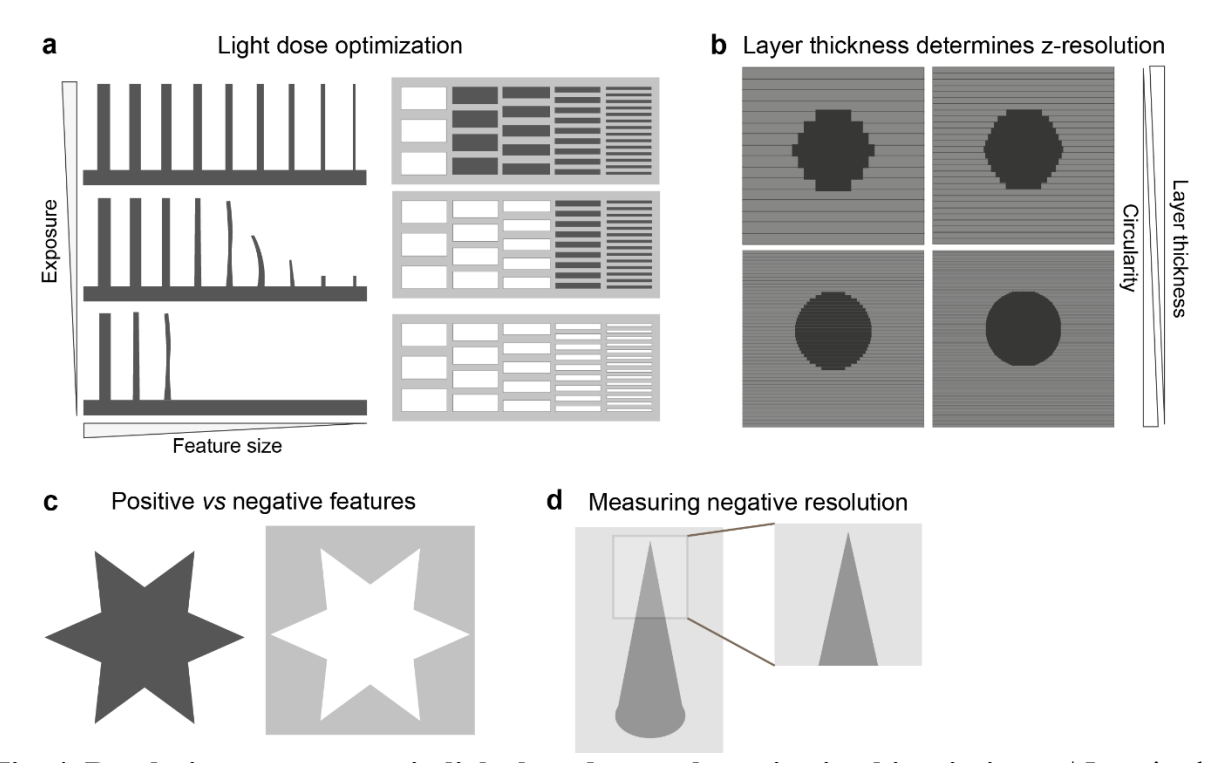


Fig. 4. Resolution assessments in light-based vat-polymerization bioprinting. a | In point-by-point and layer-by-layer vat-polymerization, resolution is assessed by printing diagnostic models with small positive and negative features that range in size at light-exposure parameters in the optimal range of identified with the working curve. **b** | In SLA/DLP the printed structures can display a notable pixelated profile depending on the layer thickness. **c** | Tomographic bioprinting enables fabrication of objects in a layerless fashion with the resolutions measurable through attainable negative and positive features. **d** | Measurement of the resolution of negative features can be facilitated by using fluorescent dyes; here a negative cone is filled with a dye, and the maximum attainable negative resolution is determined by measuring the tip dimensions of the cone.

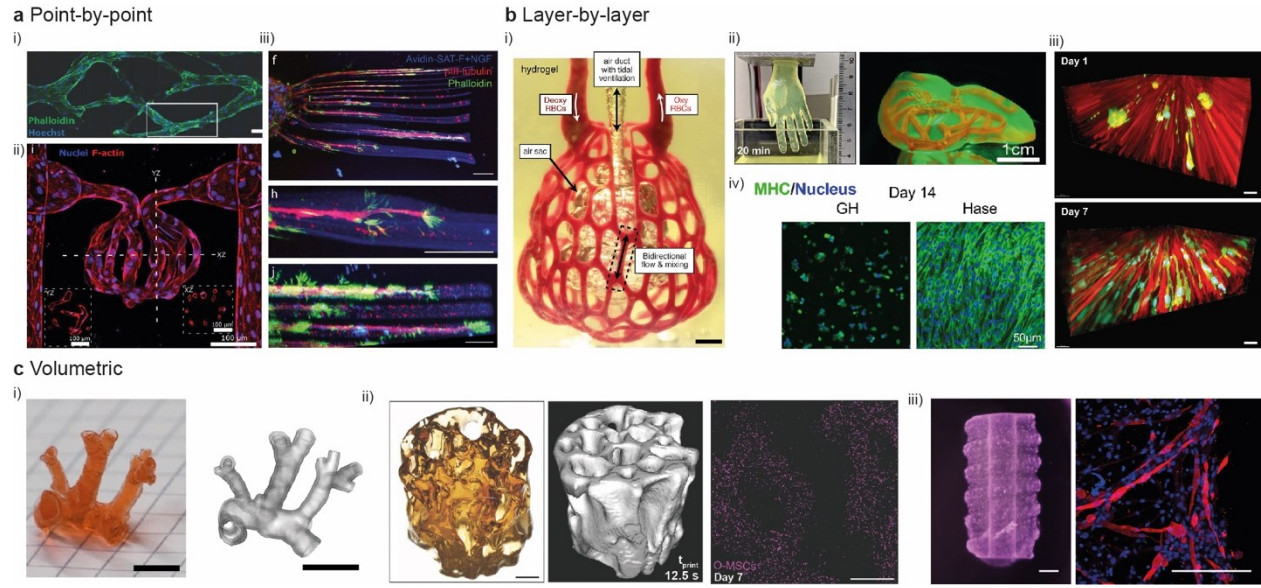


Fig. 5 | **Examples of tissue engineered constructs. a** | Point-by-point printing of vascular network by means of TPL with HUVECs endothelialization (i). Two-photon-based ablation and endothelialization of glomerulus-like vasculature (ii). Reproduced with permission from Ref. ¹⁶⁶. Two-photon patterning of growth factors to guide axon outgrowth (iii). Scale bars: 50 μm. Reproduced with permission from Ref. ¹⁶¹. **b** | Layer-by-layer printing of entangled vasculature networks (i). Scale bar: 1 mm. Reproduced with permission from Ref. ¹⁴⁶. Fast printing of large constructs featuring perfusable channels (ii). Reproduced with permission from Ref. ¹⁹⁷. Cellular alignment in FLight-bioprinted constructs (iii). Scale bars: 20 μm. Reproduced with permission from Ref. ²¹⁰. Differentiation of C2C12 muscle cells in bioprinted constructs without (stiff gel, GH) or with (soft gel, Hase) enzymatic digestion (iv). Reproduced with permission from Ref. ¹¹³. **c** | High-fidelity tomographic printing of mouse pulmonary artery (i), bioprinting of MSC-laden trabecular bone (ii) and C2C12 myoblast-laden complex model (iii). Scale bars: 5 mm/5 mm (i), 2 mm/500 μm (ii), and 2 mm/200 μm (iii). Reproduced with permission from Refs. ^{33,83,149}.

6 .	sox 1 Typical bioresin formulations for fight-based vat-polymerization bioprinting.
7 8	Hydrogel network materials
9	Poly(ethylene glycol)-diacrylate
)	• Pluronic-F127
	Poly(vinyl alcohol)
	Hyperbranched polyglycerol
	 Decellularized extracellular matrix and derivatives
	Gelatin and derivatives
	Hyaluronic acid and derivatives
	Collagen and derivatives
	• Silk and derivatives
	Alginate and derivatives
	Photocrosslinking chemistries
	Acrylate/methacrylate chain polymerization
	Thiol-ene and thiol-yne step-growth polymerization
	Photooxidative tyrosine-dimerization
	• Initiator-free photoligation (e.g., coumarin dimerization, diazonium photolysis)
	Photoclick network conjugation of guest-host crosslinks
	The control from the figures of Boses from the control fr
	Small molecules & additives
	• Photoinitiators (e.g., I2959, LAP, Eosin Y, Ru/SPS, upconverting nanoparticles)
	• Absorbers (e.g., to limit light penetration or scattering)
	• Inhibitors (e.g., scavengers, quenchers)
	• Refractive index-modifiers (e.g., iodixanol)
	• Nanocomposite components (e.g., graphene, silica)
	Special considerations
	Ionic, hydrogen bonding, or thermoresponsive components
	Dynamic, responsive, or degradable macromers or crosslinkers
	Photocaged reactive groups
	Simultaneous preparation of interpenetrating networks
	 Multi-material approaches (bioresin switching, overprinting, bioresin orthogonality, etc.)
	• Computed light dose gradient for scattering correction
	• Post-printing cell-material interactions (e.g., network-softening or contraction)
	r
	Box 2. Recommended key parameters of light-based vat-polymerization bioprinting that
,	hould be reported to maximize reproducibility.
-	Bioresins (biomaterials)
	• Type of biomaterial

• Origin of biomaterial

- Biomaterial concentration
 - Catalog or lot number of biomaterial if commercially sourced
 - Procedures for synthesis, derivation or modification of biomaterials if manufactured inhouse
 - Pertinent information regarding photoinitiators

1638

1639

1640

1641

1642

1632

1633 1634

Bioresins (cells)

- Type of cell or cells
- Catalog or lot number of cells
- Cell culture medium and conditions
- Passage number
- Cell density
- Procedures for isolation, modification, or differentiation of cells if applicable

1643 1644

1646

1647

Bioprinter hardware and software

- Type/model
- Sub-type
- Bioresin/vat temperature
- Specifics for DiY or modification if applicable

1649 1650

1652

1655

1656

1657

1658

Bioprinting procedure

- Raster-scanning step size (TPL/SLA) or projection pixel size (DLP/VAM)
- Raster-scanning speed (TPL/SLA), layer projection time (DLP), or vat rotation speed (VAM)
- Layer thickness (TPL/SLA/DLP) or vat rotation step angle (tomographic printing)
- Details of software used for segmentation and planning the bioprinting path; specify if custom-designed
- Ambient temperature if different than that of bioresin/vat
- Other photocrosslinking or photodegradation parameters, including laser/light output power density and wavelength used. If multiple procedures are used (such as in multimaterial), specific information of each procedure

1662 1663

1664

1665

Post-bioprinting

- Tissue culture conditions
- Maturation conditions
- Specifics on culture medium, culture container, and other culture conditions
- Type and specifics of the maturation methods if applicable (e.g., flow, biomechanical, bioelectrical)

 $Table\ 1\ |\ Key\ performance\ indicators\ for\ vat-polymerization\ bioprinting\ techniques.\ The\ data\ refer\ to\ prints\ with\ cells\ but\ not\ acellular\ constructs.$

Bioprinting technique	Minimum feature size	Bioresin Viscosity	Modulus range	Time to build 1- cm ³ constructs
Extrusion	~100 µm ²³⁶	$0.005 – 100 \; Pa \; s^{237}$	1–200 kPa ^{238,239}	Minutes-hours
TPL	2–8 μm ^{157,161}	>10 Pa s ²⁴⁰	$0.1-140 \text{ kPa}^{143,241}$	Hours
SLA	5–10 μm ^{242,243}	$0.25{-}10~{\rm Pa}~{\rm s}^{87}$	2-20 kPa ^{146,244}	Minutes-hours
DLP	10–50 μm ^{30,114}	$0.25{-}10~{\rm Pa}~{\rm s}^{87}$	1-180 kPa ^{113,114}	Minutes
VAM	~40 µm ³³	>10 Pa s ³⁷	$0.4-25 \text{ kPa}^{33,83}$	Seconds

Supplementary Information 1673

1674

Light-based vat-polymerization bioprinting

1675 1676

Riccardo Levato^{1,2,†} Oksana Dudaryeva², Carlos Ezio Garciamendez-Mijares³, Bruce E. 1677 Kirkpatrick^{4,5,6}, Riccardo Rizzo⁷, Jacob Schimelman⁸, Kristi S. Anseth^{4,5}, Shaochen Chen⁸, Marcy 1678 Zenobi-Wong⁷, Yu Shrike Zhang^{3,†} 1679

1680

1693

- ¹Department of Clinical Sciences, Faculty of Veterinary Medicine, Utrecht University, Utrecht, 1681 The Netherlands 1682
- ²Department of Orthopedics, University Medical Center Utrecht, Utrecht, The Netherlands
- ³Division of Engineering in Medicine, Brigham and Women's Hospital, Department of Medicine, 1684
- Harvard Medical School, Cambridge, MA 02139, USA
- ⁴Department of Chemical and Biological Engineering, University of Colorado Boulder, Boulder, 1686 CO 80303, USA 1687
- ⁵BioFrontiers Institute, University of Colorado Boulder, Boulder, CO 80303, USA
- ⁶Medical Scientist Training Program, University of Colorado Anschutz Medical Campus, Aurora 1689 CO 80045, USA 1690
- ⁷Department of Health Sciences and Technology, ETH Zürich, Zürich, Switzerland
- ⁸Department of NanoEngineering, University of California San Diego, La Jolla, CA 92093, USA 1692

†Emails: r.levato@uu.nl (R. L.); yszhang@research.bwh.harvard.edu (Y. S. Z.) 1694



Fig. S1 | Illustrations of the different digital model slicing algorithms in vat-polymerization bioprinting. a | Point-by-point method (SLA/TPL). b | Layer-by-layer method (DLP). \mathbf{c} | Volumetric method (VAM).

 $Table \ S1 \mid Examples \ of software \ options \ for \ the \ different \ steps \ of \ the \ vat-polymerization \ 3D \ bioprinting \ process.$

Software	General ability and use purpose
Voxelizer	
, oxerger	MATLAB
	Open-source (MATLAB license required)
<u>3D voxelizer</u>	OBJ files supported as input
	Resolution can be adjusted
	C++
	Open-source
<u>cuda_voxelizer</u>	Several file formats supported as input including STL and OBJ
	OBJ files supported as output
	Utilizes GPU instead of CPU
	C/C++
<u>FastVoxel</u>	Open source PLY files supported as input
<u>rast v oxer</u>	Easily installed with a Python script
	Resolution can be adjusted
	MATLAB
	Open-source (MATLAB license required)
Mesh voxelisation	Several file formats supported as input; including STL
	Several file formats supported as output
	Resolution can be adjusted
	C++
1.0	Open-source
obj2voxel	STL or OBJ files supported as input
	Several file formats supported as output including PLY
	Resolution can be adjusted Python
	Open-source
polydata to imagedata	STL or PLY files supported as input
pory data_to_magedata	VTI files supported as output
	Resolution can be modified
	Python
PyVoxelizer	Open-source
1 y v Oxelizer	STL, OBJ, and MTL files supported as input
	Resolution can be adjusted
	Python
	Open-source
stl-to-voxel	STL files supported as input Several file formats supported as output; PNG, XYZ, and SVX
	Color voxelization (output) possible
	Resolution can be adjusted
	Python
V1:4:	Built-in function of the NURBS-Python library
Voxelization	OBJ files supported as input
	Resolution can be adjusted
	C++
1 10	Open-source
voxelization_and_sdf	PLY files supported as input
	Color voxelization (input and output) possible Resolution can be adjusted
	C++
	Open-source
voxelizer	STL and OBJ files supported as input
	XML files supported as output
	Resolution can be adjusted
	C/C++
voxelizer	Open-source
	OBJ files supported as input

	Resolution can be adjusted
	C++
	Open-source
<u>Voxelizer</u>	STL, PLY, and 3DS files supported as input
	Resolution can be adjusted
	JavaScript
	Open-source
Voxelizer	STL, OBJ, and gITF supported as inputs
	XML files supported as output
	Resolution can be adjusted
Slicing algorithm	
	DLP
D:14D	Closed-source; license requires
BuildBee	Several file formats supported as input including STL and OBJ Specific 3D printers supported
	Advanced UI and options
	VAM
	Open-source (MATLAB license required)
CAL-software	STL files supported as input
	Slicing and host projection software
	Advanced slicing algorithm implemented
	SLA/DLP
	Closed-source; free and license versions available
<u>Chitubox</u>	Several file formats supported as input including STL
	Specific 3D printers supported; works in conjunction with custom firmware
	Advanced UI and options DLP
	Closed-source; free version
Creation Workshop	Designed to work as a host firmware
<u> creation workshop</u>	Several file formats supported as input including STL and OBJ
	Interactive UI
	TPP
	Closed-source; license required
DeScribe	STL files supported as input
	Specific 3D printer supported
	GWL files supported as output Advanced UI and options with adaptive slicing
	SLA/DLP
	Closed-source; license required
E 2D	Several file formats supported as input including STL, OBJ, and PLY
Formware 3D	Several file formats supported as output
	Generic and specific 3D printers supported
	Advanced UI and options
	DLP
11-4	Open-source; JavaScript
hackathon-slicer	STL files supported as input PNG files supported as output
	Interactive UI and hosted version also available
	TPP
	Closed-source; license required
Luminis	Specific 3D printer supported
	Integrated slicer and host controller
	Advanced UI and options
	SLA/DLP
Lychee Slicer	Closed-source; free and license versions available
	Specific 3D printers supported
	Advanced UI and options DLP
	Open-source; Python
monkeyprint	Designed to work as a host firmware
	STL files supported as input

	Interactive UI
	SLA/DLP
N. DID	Closed- and open-source versions available
<u>NanoDLP</u>	Designed to work as a host firmware on a Raspberry Pi
	Advanced UI and options
	SLA/DLP
	Open-source; C++
D CI'	STL, OBJ, and AMF files supported as input
Prusa Slicer	PNG files supported as output
	Color slicing supported
	Advanced UI and options
	SLA/DLP
	Closed-source; free version
Slic3r	Ability to add custom C++ applications
	SVG files supported as output
	Interactive UI
	DLP
	Open-source; Python
stl-to-voxel	STL files supported as input
	PNG, XYZ, and SVX supported as output
	Color slicing supported
	TPP
	Closed-source; license required
THINK3D	STL files supported as input
11111 11100	Specific 3D printer supported
	Integrated slicer and host controller; real-time viewing/printing
	Advanced UI and options
	VAM
X 4 3 6 7 11	Open-source; Python
VAMToolbox	STL files supported as input
	Slicing and host projection software
	Advanced slicing algorithm implemented DLP
Voxeldance Tango	Cloused-source; license required Specific 3D printers supported
	Advanced UI and options DLP
	Closed-source; free version
Z-suite	Several file formats supported as input including STL and OBJ
<u>Z-suite</u>	Specific 3D printers supported
	Advanced UI and options
CAD, computer-aided design: UI: user interface	Travances of and options

CAD, computer-aided design; UI: user interface